

BIT INTERLEAVED CODED SPATIAL MODULATION

by

Furkan Kerim Kadi

B.S., Electronics and Communication Engineering, Yıldız Technical University, 2011

Submitted to the Institute for Graduate Studies in
Science and Engineering in partial fulfillment of
the requirements for the degree of
Master of Science

Graduate Program in Electrical and Electronics Engineering
Boğaziçi University

2019

ACKNOWLEDGEMENTS

First of all, I would like to thank to my advisor Prof. Mutlu Koca for his support and remarkable advices during my study in Boğaziçi University. Without his encouragement, help and guidance this thesis would not be accomplished.

I thank my jury committee members Prof. Emin Anarım and Prof. Erdal Panayırıcı for their constructive advices and insightful comments at my thesis defence.

I would like to express my gratitude to all members of WCL, for their warm and friendly environment.

Last but not least i am deeply grateful to my parents Şaban and Zeynep Kadı and my sister Şeyma Kadı for their eternal love and support. This thesis is dedicated to the memory of my father, who is also my teacher, inspired scientific thinking in my life and to my mother who always provided encouragement and unfailing support.

This thesis is supported by the Scientific and Technological Research Council of Turkey (TUBITAK) under the grant number 111E274.

ABSTRACT

BIT INTERLEAVED CODED SPATIAL MODULATION

Spatial modulation is a novel modulation technique that utilize antenna space in addition to symbol space for information transmission. This technique is implemented with the well known BICM system to provide robustness and better error protection. This thesis focus on two main problems, how much coding is required for antenna and symbol bits and how equal or unequal coding strategies can be implemented to perform better on various channel conditions. To determine amount of required protection for antenna and symbol bits a new metric is developed. This metric also provide insight for system design in different channel conditions and for required coding strategies. Moreover, an upper bounding technique is developed for performance evaluation of both BICSM-EEP and BICSM-UEP systems with hard decision decoding. This technique is used for performance comparison of different coding schemes in various channel conditions and to develop best punctured code selection mechanism. Punctured convolutional codes are one of the most vital part of both BICSM-EEP and BICSM-UEP systems and because of that, their effect on implementing EEP or UEP coding strategies are well investigated. Finally observations about factors that affect overall system performance of EEP and UEP systems are presented in light of comparative performance analysis.

ÖZET

BİT SERPİŞTİRMELİ KODLAMALI UZAMSAL KİPLEME

Uzamsal kiplenim bilgi aktarımında sembol uzayının yanı sıra anten uzayından da faydalanan yeni geliştirilmiş bir tekniktir. Bu teknik daha iyi hata koruması ve dayanıklılık elde etmek için sıklıkla kullanılan BICM sistemiyle birlikte uygulanmıştır. Bu tez kapsamında anten ve sembol bitleri için ne kadar kodlama gerektiği ve farklı kanal koşullarında eşit ve eşit olmayan kodlama stratejilerinin daha iyi başarımlar sağlamak için nasıl uygulanacağını içeren iki ana probleme odaklanılmıştır. Anten ve sembol bitleri için gerekli olan koruma miktarını belirlemek için yeni bir ölçev geliştirilmiştir. Bu ölçev aynı zamanda farklı kanal koşullarında sistem tasarımı ve gereken kodlama stratejileri için kavrayış sağlar. Ayrıca, BICSM-EEP ve BICSM-UEP sistemlerinde sıfır bir kararlı kod çözme durumunda başarımların değerlendirilmesi için bir üst sınırlama tekniği geliştirilmiştir. Bu teknik, çeşitli kanal koşullarında farklı kodlama şemalarının başarımlarının karşılaştırılmasında ve en iyi delikli kod seçim yöntemi geliştirilmesinde kullanılmıştır. Delikli evrişimli kodlar BICSM-EEP ve BICSM-UEP sistemlerinin en önemli parçalarından biridir ve bundan dolayı eşit/eşit olmayan kodlama stratejileri uygulamasındaki etkileri araştırılmıştır. Son olarak BICSM-EEP/UEP sistemlerinde genel sistem başarımlarını etkileyen unsurlar hakkında karşılaştırmalı başarımların analizi ışığında yapılan gözlemler sunulmuştur.

TABLE OF CONTENTS

ACKNOWLEDGEMENTS	iii
ABSTRACT	iv
ÖZET	v
LIST OF FIGURES	viii
LIST OF TABLES	xi
LIST OF SYMBOLS	xii
LIST OF ACRONYMS/ABBREVIATIONS	xv
1. INTRODUCTION	1
1.1. Spatial Modulation	1
1.2. BICM and BICSM	3
1.3. UEP BICSM	5
1.4. Outline	6
2. SYSTEM MODEL	7
2.1. Signal Model	7
2.2. Channel Model	8
2.3. SM Optimal Detection and Uncoded Average Probability of Error	10
2.3.1. Rayleigh Fading	12
3. EQUAL AND UNEQUAL ERROR PROTECTION STRATEGIES	14
3.1. Uncoded SM Antenna and Symbol Bits Comparison	14
3.2. Quantification of Error Protection with New Metric	16
4. DESIGN AND PERFORMANCE ANALYSIS OF BICSM EEP/UEP	19
4.1. Equal Error Protection BICSM Design and Performance Analysis	19
4.2. Upper Bound Derivation for BER Performance of BICSM-EEP	20
4.3. Best Punctured Convolutional Code Search for EEP	21
4.4. Simulation Results for EEP	27
4.5. Unequal Error Protection BICSM Design and Performance Analysis	29
4.6. Upper Bound Derivation for BER Performance of BICSM-UEP	31
4.7. Best Punctured Convolutional Code Search for UEP	32

4.8. Comparative Performance Analysis of BICSM-EEP and BICSM-UEP Systems	36
5. SOFT DECISION DECODING	42
5.1. Soft Decision Decoding System Model	42
5.2. Simulation Results for Soft Decision Decoding	43
6. CONCLUSION	47
REFERENCES	49

LIST OF FIGURES

Figure 2.1.	Block diagram of BICSM transceiver system.	7
Figure 3.1.	Uncoded Antenna and Symbol Bits Performance over Rayleigh Fading Channels.	15
Figure 3.2.	Uncoded Antenna and Symbol Bits Performance over Rician Fading Channels.	15
Figure 3.3.	Transmit Correlation effects on P_b^a/P_b^s	17
Figure 3.4.	Rician coefficient K vs P_b^a/P_b^s	18
Figure 3.5.	Rician Fading Channels with various K values vs P_b^a/P_b^s	18
Figure 4.1.	Block diagram of BICSM-EEP transmitter system.	19
Figure 4.2.	Block diagram of BICSM-EEP receiver system.	20
Figure 4.3.	EEP scheme BER performance in Rayleigh fading channels with one bit puncturing pattern.	23
Figure 4.4.	EEP scheme BER performance in Rician fading channels with one bit puncturing pattern.	24
Figure 4.5.	EEP scheme BER performance in Rayleigh fading channels with two bits puncturing pattern.	24

Figure 4.6.	EEP scheme BER performance in Rician fading channels with two bits puncturing pattern.	25
Figure 4.7.	EEP scheme BER performance in Rayleigh fading channels with three bits puncturing pattern.	25
Figure 4.8.	EEP scheme BER performance in Rician fading channels with three bits puncturing pattern.	26
Figure 4.9.	EEP scheme performance simulation and upper bound in Rayleigh Fading Channels with various puncturing pattern.	28
Figure 4.10.	EEP scheme performance simulation and upper bound in Rician fading channels with various puncturing pattern.	29
Figure 4.11.	Block diagram of BICSM-UEP transmitter system.	29
Figure 4.12.	Block diagram of BICSM-UEP receiver system.	30
Figure 4.13.	UEP scheme in Rayleigh fading channels with one bit puncturing.	34
Figure 4.14.	UEP scheme in Rician fading channels with one bit puncturing.	34
Figure 4.15.	UEP scheme in Rayleigh fading channels in two bits puncturing pattern.	35
Figure 4.16.	UEP scheme in Rician fading channel with two bits puncturing pattern.	35
Figure 4.17.	EEP/UEP BER performances in uncorrelated/correlated Rayleigh fading channels with various puncturing patterns.	38

Figure 4.18.	EEP/UEP BER performances in uncorrelated/correlated Rician fading channels with various puncturing patterns.	40
Figure 5.1.	Block diagram of SISO BICSM-EEP receiver system.	42
Figure 5.2.	Block diagram of SISO BICSM-UEP receiver system.	43
Figure 5.3.	Soft Decoded Rayleigh Fading Channels with various puncturing pattern.	45
Figure 5.4.	Soft Decoded Rician Fading Channels with various puncturing pattern.	45

LIST OF TABLES

Table 4.1.	EEP Weight Distribution $n = 2, \bar{K} = 3, p = 4, (5, 7)$	26
Table 4.2.	EEP Weight Distribution $n = 2, \bar{K} = 5, p = 4, (23, 35)$	27
Table 4.3.	UEP Weight Distribution $n = 2, \bar{K} = 3, p = 3, (5, 7)$	36
Table 4.4.	UEP Weight Distribution $n = 2, \bar{K} = 5, p = 3, (23, 35)$	36

LIST OF SYMBOLS

c	Coded interleaved bit sequence
c_a	Coded antenna bits
c_s	Coded symbol bits
c_j	Interleaved coded bit sequence elements
C_d	Convolutional code weighting coefficients
\mathcal{CN}	Complex Gaussian random variable
\hat{c}_a	Received coded antenna bit sequence
\hat{c}_s	Received coded symbol bit sequence
d	Hamming distance
d_{free}	Minimum free distance of convolutional code
E	Expected value
h_u	u -th column of channel matrix H
χ_v	v -th element of modulation alphabet χ
$h_{\hat{u}}$	\hat{u} -th column of channel matrix H
H	Channel matrix
\tilde{H}	Variable part of channel matrix
\bar{H}	Fixed part of channel matrix
k	k input of convolutional code
K	Rician coefficient
\bar{K}	Constraint length of convolutional code
$L_a(v)$	Deinterleaved decoded bit sequence
$L_a(v_a)$	Deinterleaved decoded antenna bit sequence
$L_a(v_s)$	Deinterleaved decoded symbol bit sequence
$L_a(c_a)$	Antenna code LLR
$L_a(c_s)$	Symbol code LLR
$L_a(c)$	Interleaved code LLR
$L_e(c)$	Received coded bit sequence
$L_e(c_a)$	Received coded antenna bit sequence

$L_e(v)$	Code LLR
$L_p(u)$	Decoded bit sequence
$L_p(c_{a,i})$	LLR with antenna bits
$L_p(c_{s,i})$	LLR with symbol bits
m	Number of symbol bits
M	Symbol constellation size
m_z	Mean vector
\tilde{m}_z	Half of mean vector m_z
n	Number of antenna bits
N_0	Noise spectral density
N_t	Number of transmit antennas
N_r	Number of receive antennas
p	Puncturing period
P	Puncturing matrix
P_b	Uncoded system bit error probability
P_b^s	Uncoded symbol bit error probability
P_c^a	Coded antenna bit error probability
P_b^a	Uncoded antenna bit error probability
P_c^s	Coded symbol bit error probability
P_d	First event error probability
P_d^a	First event error probability of antenna bits
P_d^s	First event error probability of symbol bits
$\bar{P}_s^{\text{Rayleigh}}$	APEP in uncorrelated Rayleigh fading case
R	Code rate
u	Antenna index
u_{ML}	Optimum antenna index with maximum likelihood sense
$U_{i,1}$	Antenna index subset where i-th element is 1
$U_{i,0}$	Antenna index subset where i-th element is 0
\hat{u}	Received antenna index estimate
v	Symbol index
v_{ML}	Optimum symbol index with maximum likelihood sense

$V_{i,1}$	Symbol index subset where i-th element is 1
$V_{i,0}$	Symbol index subset where i-th element is 0
\hat{v}	Received symbol index estimate
α	Correlation coefficients between adjacent antennas
α^r	Receive correlation coefficient
α^t	Transmit correlation coefficient
λ_k	k-th eigenvalue of matrix
ξ_k	k-th residual in the partial fraction expression
Π	Interleaver
σ^r	Elements of receive correlation matrix
σ^t	Elements of transmit correlation matrix
χ	Modulation symbol set
Σ_t	Transmit correlation matrix
Σ_r	Receive correlation matrix
Σ_z	Covariance matrix of vector z

LIST OF ACRONYMS/ABBREVIATIONS

4G	4-th Generation
ABEP	Average Bit Error Probability
APEP	Average Pairwise Error Probability
AWGN	Additive White Gaussian Noise
BER	Bit Error Rate
BICM	Bit Interleaved Coded Modulation
BICSM	Bit Interleaved Coded Spatial Modulation
BICSM-EEP	Bit Interleaved Coded Spatial Modulation with Equal Error Protection
BICSM-UEP	Bit Interleaved Coded Spatial Modulation with Unequal Error Protection
BIOS	Binary Input Output Symmetric
BSC	Binary Symmetric Channel
CSM	Coded Spatial Modulation
DSL	Digital Subscriber Line
DVB-S2	Digital Video Broadcasting Satellite Second Generation
EEP	Equal Error Protection
IAS	Inter Antenna Separation
ICI	Inter Channel Interference
ICT	Information and Communication Technology
ID	Iterative Decoding
LAN	Local Area Network
LLR	Log Likelihood Ration
LOS	Line of Sight
L-value	Log Likelihood Ratio
MAP	Maximum a Posteriori Probability
MIMO	Multiple Input Multiple Output
ML	Maximum Likelihood
OFDM	Orthogonal Frequency Division Multiplexing

PDF	Probability Density Function
PEP	Pairwise Error Probability
PSK	Phase Shift Keying
QAM	Quadrature Amplitude Modulation
QPSK	Quadrature Phase Shift Keying
RF	Radio Frequency
SISO	Soft Input Soft Output
SM	Spatial Modulation
SM-TC	Spatial Modulation with Trellis Coding
SNR	Signal to Noise Ratio
SSK	Space Shift Keying
TCM	Trellis Coded Modulation
TCSM	Trellis Coded Spatial Modulation
UEP	Unequal Error Protection

1. INTRODUCTION

From the last decade number of subscribers that demand wideband wireless system connection tremendously increased by the introduction of bandwidth hungry mobile devices and applications. This increase brings the key challenge of more spectrally efficient communication system designs. On the other hand another big challenge of today's and future's mobile communication systems is energy efficiency. As stated in [1] for the year 2014, the ICT sector represents around 2% of the global carbon emissions, of which mobile networks contribute about 0.2%. This is comparable to the worldwide carbon emissions of airplanes, and about a quarter of the worldwide carbon emissions of cars. Furthermore, this amount is expected to increase every year at a rapid pace due to the massive increase of the mobile data traffic. As an approach to solve this problem, an energy efficient technique for communication, spatial modulation offered in [2,3].

1.1. Spatial Modulation

Spatial modulation [2] is an emerging multi antenna technique that information conveyed both signal and antenna space. Compared to other multi antenna techniques [4] in SM system only one antenna is activated at any time instance. This provides significant simplification of transceiver system and drawbacks of MIMO such as ICI, IAS and need of multiple RF chains avoided. Reduced number of RF chains also make SM system more energy efficient.

The key feature of SM is to map incoming information bits to two information carrying units, symbol from a modulation alphabet and transmit antenna index. So that at any given time instant two different type of information is transmitted together. When information carrying unit is only antenna indexes it turns into another technique called SSK [5] modulation. Since SSK only uses antenna space it has simpler receiver structure. In SM, information divided in two sub stream, former is mapped to antenna index positions and later is mapped to symbols. Then, symbol is transmitted through a

channel with only one antenna active at a time. Here, channel plays an important role, propagation environment has imperfections and it affects transmitted signals differently owing to different spatial positions of antennas. And so that every transmission channel between transmit and receive antenna has a unique fingerprint of channel effects. This is fundamental working principle of SM system, which makes detection of active antenna index at the receiver possible. Optimal detection for SM system introduced in [6]. At the receiver channel state information is required to make detection possible. In practice this can be obtained by channel estimation. In total $N_t N_r$ channel impulse response has to be estimated. Method presented in [6] uses ML principle in which Euclidean distances between received and set of possible signals computed and closest one is chosen. Total number of $M N_t N_r$ euclidean distances has to be calculated for comparison.

There are several advantages of SM system [7]. The use of single RF chain completely avoids ICI and IAS. Also SM system can achieve multiplexing gain proportional to number of antennas. But the increase in spectral efficiency via antennas is limited to $\log_2(N_t)$ and it is not linearly increased with antenna number likewise MIMO. Spectral efficiency could be increased by using concept of generalized spatial modulation proposed in [8]. In that work proposed method is, using subset of antennas instead of one. That increase possible number of antenna constellation size but that concept is out of scope of this thesis. SM can effectively work in cases receive antenna number lesser than transmit antenna number. Even the one receive antenna can be used. This property is especially useful in wireless communication because mobile devices have limited space for high number of antennas. SM's advantages have created a growing interest in a wide range of SM-based MIMO communications system, including the possible extension to ultra-wide band communication which stated with SSK and SM in [9–11]. Moreover, SM technique is extended to indoor optical communication in [12]. In [13] the authors combined SM and Alamouti space-time block code STBC and demonstrate that multiplexing and diversity gains can be achieved.

Performance analysis of spatial modulation widely studied in literature. One of the first work in this area is [14]. Although it gives important insight of performance

evaluation, analysis lacks of different channel conditions and modulation schemes. Then in [15] a general framework for SM performance presented for correlated fading channels and for any constellation size. SM performance at correlated and uncorrelated Nakagami fading channel proposed in [16]. Comparative analysis of SM performance with OFDM system made in [17].

Idea of coded spatial modulation is also studied in the literature. Trellis coded modulation is introduced in [18] to reduce effects of channel. It is observed that presence of LOS component, which is modelled with Rician fading and heavy transmit correlation have more detrimental effect on antenna bits. Although this method provides some protection for antenna bits, it increases symbol constellation size and left symbol bits unprotected. To solve this problem in [19], SM with trellis coding presented where all incoming bits are encoded and coded bits mapped on to antenna and symbol indices. Nevertheless the number of trellis states required to be at least double for each increment in spectral efficiency and this makes this technique impractical for high data rate applications. A novel approach BICSM is also addressed in [20]. Compared to other coding techniques, proposed method is more flexible which is not just limited to particular class of trellis codes or being effective in certain channel conditions. And also even further performance gain obtained using iterative decoding techniques.

1.2. BICM and BICSM

Coded modulation is a technique that merges coding and modulation in a single entity to get a bandwidth efficient scheme. One of the first concept in this field is proposed pioneering work of Ungerboeck in [21], is called TCM. TCM system is based on combination of convolutional code and discrete signal constellation. Later, BICM was first introduced in the well known study of Zehavi [22] in order to provide improvement over diversity order of TCM. BICM system consist of serial concatenation of convolutional encoder, bit by bit interleaver and high order modulation. Bit interleaving makes span of error event to extend. And also interleaving spreads bit errors to many channel symbols so BICM actually increases time diversity of coded bits and this increases the performance. Signal labelling [23] is another important aspect of BICM

since it also affect system performance. Maximum likelihood decoding of BICM system is too complex to implement because joint decoding and demodulation is required. Instead, a suboptimal method suggested by Zehavi [22] that using bit metric calculation and viterbi decoding. Bit interleaved coded modulation with iterative decoding proposed by Li and Ritcey [24, 25] for further improvement of BICM performance. They showed in [24] with implementing large block length, ID performance asymptotically approaches the performance of error free feedback bound.

BICM characteristics was extensively studied in an information theory viewpoint by Caire et al [26] and authors showed that BICM channel is actually behaves like memoryless BIOS channel. They also proposed BICM union and expurgated bounds for bit error rate analysis of BICM systems. A tighter bound for square QAM and gray labeling case is offered in [27]. As another aspect an algorithmic method to calculate closed form expression for PDF of L-values in BICM system offered in [28] while PDF of L-values is an important parameter for calculation of coded system performance. But the system suggested in [28] only includes unfaded channel conditions. Although all these upper bounding techniques gives an approximation to system behaviour they are rather loose or limited to certain modulation scheme and channel conditions. Alternatively an approach for error probability analysis of BICM, PEP calculation using saddle point approximation is proposed in [29]. This technique is simpler compared to previous upper bounding techniques. Moreover a good study about saddle point technique can be found in [30] and its application to different channel conditions and symbol constellations.

Advantages of BICM system is listed in [31] as, it's flexibility, robustness, negligible losses in scalar channels and increased diversity. BICM allows the designer to choose constellation and coding scheme independently. BICM flexibility is so high that it can be implemented cases such as modulation varies within a symbol period or coding puncturing varies with block of bits [32]. This property is especially useful in wireless communication because it enables to fit intended rates to channel conditions. Robustness of BICM came with decoder design only with one parameter, the rate, can be adjusted to overcome channel variations. BICM performance loss is negligible in prac-

tical communication environment. Thanks to BICM interleaving, when transmitting information over fading channels L-values used in decision process affected by different channel realizations. This property is one of the key property of BICM system and called transmission diversity. Although these advantages BICM also has some drawbacks such as suboptimal decoding and long delays because of long interleavers. Effects of these disadvantages are negligible in practical communication. BICM is broadly employed contemporary communication systems such as DVB-S2, wireless LAN, DSL, cellular networks (4G) etc.

Powerful features and different worlds of SM and BICM combined and presented in [20]. This novel approach is called BICSM. BICSM is an effective method not only for protection of channel fading and noise but also for robustness against spatial correlations and LOS. Implementation of BICSM system is rather easy via using simple punctured convolutional codes to provide different levels of protection. BICSM has some great advantages over other CSM schemes. While TCSM [18] provides protection for antenna bits by increasing symbol alphabet (higher order modulation), it left symbol bits unprotected. And also increasing modulation alphabet size cause degradation in system performance even in some cases uncoded system overcome TCSM. BICSM similar to SM-TC [19] can provide error correction for both antenna and symbol bits. Hence, BICSM system outperform uncoded SM system in practical BER level and provides substantial performance gains. BICM implemented with same design parameters also provides performance improvement over SM-TC. Although every increment in spectral efficiency doubles trellis code complexity in SM-TC, BICSM can be implemented even 2 state codes with every spectral efficiency. Block or convolutional codes can be used as a coding scheme. In addition to that while TCSM is severely unequal error protection scheme and SM-TC is always equal error protection method BICM can easily be tailored to serve as equal or unequal protection.

1.3. UEP BICSM

BICSM is a very flexible system and can be designed to serve both EEP and UEP in certain conditions. Main focus of this thesis is extension of BICSM approach

to have an unequal error protection scheme. In [18] the authors made the observation that bits mapped on to the antenna indices requires more protection in the case of heavy channel conditions such as Rician fading where a direct LOS component is present and spatially correlated Rayleigh fading channels where the transmit correlation effects are severe. This gives insight, reasoning and possible advantages of employing unequal error protection with BICSM in similar cases. All these cases and more will be carefully studied in following chapters.

The technique of SSK [5] is a transmission technology in which information is sent over the spatial domain, information bits are used only to be mapped onto the antenna indices and at a single time a single antenna is activated to transmit a waveform. Similar to systems which uses only the signal domain to transmit information, coded modulation could be employed to protect only one type of information. In addition, if the number of transmit antennas are not to be increased (analogous to increasing the constellation size), any error correcting scheme would decrease the spectral efficiency. Therefore error protection in SSK is out of scope of this thesis.

1.4. Outline

The rest of the thesis is organized as follows. In Chapter 2, a general system model for proposed BICSM-UEP scheme is presented. Chapter 3, presents solutions on the questions of “How much error protection is required for antenna index bits and constellation symbol bits respectively? Is more always better?” And degree of protection required for antenna and symbol bits is evaluated with different channel conditions. In Chapter 4 an analytical upper bounding technique for performance analysis of hard decision decoding is developed. By using this technique best code selection in EEP and UEP is employed. Theoretical results are compared with simulations. Chapter 5 presents soft decision decoding performance simulations for UEP and EEP BICSM. Finally, Chapter 6 gives the concluding remarks and directions for future works.

2. SYSTEM MODEL

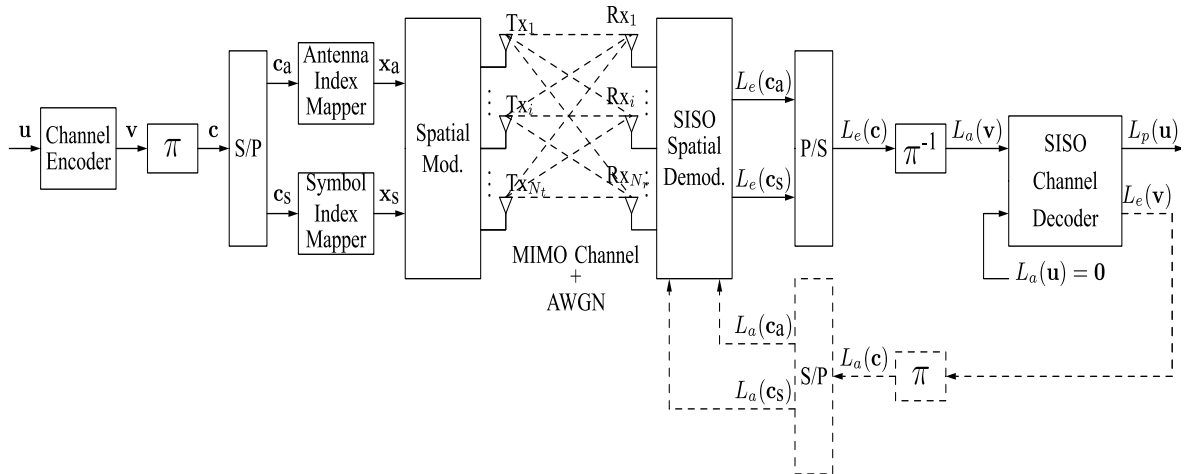


Figure 2.1. Block diagram of BICSM transceiver system.

Block diagram of BICSM transceiver scheme is shown in Figure 2.1. Firstly incoming information bits u , is encoded with convolutional encoder. Convolutional encoder output v is then interleaved by an interleaver. Then, interleaved coded sequence c is mapped to antenna indexes and symbol constellations by a mapper. Modulated symbols are transmitted through channel via only one active antenna at a time. At the channel symbols are exposed to fading, channel correlation effects and AWGN. Transmitted symbols are demodulated and demapped at spatial demodulator. Information carried by antenna indices is also extracted. This sequence is deinterleaved and deinterleaved sequence $L_a(v)$ is later decoded by the SISO channel decoder. Alternatively as shown in dotted lines L-values can be feedback to demodulator and iterative decoding can be implemented. In following subsections more detailed examination of blocks of BICSM system and signal model is presented.

2.1. Signal Model

The SM scheme is modelled by N_t transmit and N_r receive antennas employing optimum detection as in [6]. The number of transmit antennas in this scheme is an integer power of 2, i.e. $N_t = 2^n$, and the transmitter uses M -ary digital modulation to a m -bit message where $M = 2^m$ and the modulation alphabet is

$\mathcal{X} = \{ X_1, \dots, X_k, \dots, X_M \}$. $R = n + m = \log_2(N_t M)$ is the system's spectral efficiency where spectral efficiency refers to the MIMO system's transmission rate in bits/s/Hz. Each set of $n + m$ bits is divided into groups of n and m bits at each transmission moment, and the former is used to select a single transmit antenna and the latter is mapped to one of the possible M complex constellation points determined by the specific method of digital modulation. The technique used in the mapping of the bit-to-antenna index and bit-to-symbol is not in the scope of this thesis, so uniform mapping is used. The vector demonstration of the transmitted signal is $\mathbf{x} = [x_1, \dots, x_\ell, \dots, x_{N_t}]^T$ where all but one element is zero because only one antenna is active for transmission. The entries other than x_ℓ are zero and $x_\ell \in \mathcal{X}$ if the ℓ -th antenna is chosen. Namely, the non-zero element position denotes the index of the antenna and its value indicates the symbol that has been transmitted. Similar to [6], the unit power constraint, $E_x [x^\dagger x = 1]$, is assumed. This also implies a constraint of unity for the average energy of the constellation.

2.2. Channel Model

It is assumed that the MIMO channel is slow fading and generated with the sum of an average component (fixed, possibly line-of-sight - LOS) and a variable (random) component. Therefore, \mathbf{H} , $N_r \times N_t$ size channel matrix defined as;

$$\mathbf{H} = \sqrt{\frac{K}{K+1}} \bar{\mathbf{H}} + \sqrt{\frac{1}{K+1}} \tilde{\mathbf{H}} \quad (2.1)$$

where the fixed and variable components are $\bar{\mathbf{H}}$ and $\tilde{\mathbf{H}}$, respectively. K is defined as the Rician factor and the square root terms with K are the normalization weights. The $\bar{\mathbf{H}}$ is fixed part such that $[\bar{\mathbf{H}}]_{p,q} = \bar{h}_{p,q}$, for $p = 1, \dots, N_r$ and $q = 1, \dots, N_t$. The channel matrix variable component $\tilde{\mathbf{H}}$, consists of possibly correlated complex Gaussian variables. In the case of $[\tilde{\mathbf{H}}]_{p,q} = \tilde{h}_{p,q}$, for all channel coefficient pairs $(\tilde{h}_{p,q}, \tilde{h}_{\hat{p},\hat{q}})$ ($p, \hat{p} = 1, \dots, N_r$ and $q, \hat{q} = 1, \dots, N_t$) it is assumed that

$$\mathbb{E} \left[\tilde{h}_{p,q}^R \tilde{h}_{\hat{p},\hat{q}}^R \right] = \mathbb{E} \left[\tilde{h}_{p,q}^I \tilde{h}_{\hat{p},\hat{q}}^I \right], \quad (2.2)$$

$$\mathbb{E} \left[\tilde{h}_{p,q}^R \tilde{h}_{\hat{p},\hat{q}}^I \right] = \mathbb{E} \left[\tilde{h}_{p,q}^I \tilde{h}_{\hat{p},\hat{q}}^R \right] = 0. \quad (2.3)$$

That can be explained as there is no correlation between the real and imaginary parts and auto-correlations of the real and imaginary parts are the same. By using this situation, the correlated channel matrix $\tilde{\mathbf{H}}$ is defined in the Kronecker correlation model as

$$\tilde{\mathbf{H}} = \boldsymbol{\Sigma}_r^{\frac{1}{2}} \check{\mathbf{H}} \boldsymbol{\Sigma}_t^{\frac{1}{2}T} \quad (2.4)$$

where the real valued and Hermitian symmetric transmit and receive correlation matrices denoted by $\boldsymbol{\Sigma}_t$, and $\boldsymbol{\Sigma}_r$ respectively. The elements of matrices defined as $[\boldsymbol{\Sigma}_t]_{q,\hat{q}} = \sigma_{q,\hat{q}}^t$ for $q, \hat{q} = 1, \dots, N_t$ and $[\boldsymbol{\Sigma}_r]_{p,\hat{p}} = \sigma_{p,\hat{p}}^r$ for $p, \hat{p} = 1, \dots, N_r$. The Rayleigh fading channel matrix $\check{\mathbf{H}}$ consist of elements that are independent identically distributed Gaussian random complex variables i.e., $[\check{\mathbf{H}}]_{p,q} = \check{h}_{p,q} \sim \mathcal{CN}(0, 1)$ for $p = 1, \dots, N_r$ and $q = 1, \dots, N_t$.

The general channel model can be rewritten as a combination of (2.1) and (2.4);

$$\mathbf{H} = \sqrt{\frac{K}{K+1}} \bar{\mathbf{H}} + \sqrt{\frac{1}{K+1}} \boldsymbol{\Sigma}_r^{\frac{1}{2}} \check{\mathbf{H}} \boldsymbol{\Sigma}_t^{\frac{1}{2}T} \quad (2.5)$$

Which makes it possible to characterize number of channel fading situations in a single expression by selecting the suitable parameters. For instance,

- (i) $K = 0$, $\boldsymbol{\Sigma}_r = I_{N_r \times N_r}$ and $\boldsymbol{\Sigma}_t = I_{N_t \times N_t}$: Uncorrelated Rayleigh fading,
- (ii) $K = 0$, $\boldsymbol{\Sigma}_r \neq I_{N_r \times N_r}$ and/or $\boldsymbol{\Sigma}_t \neq I_{N_t \times N_t}$: Correlated Rayleigh fading,
- (iii) $K \neq 0$, $\boldsymbol{\Sigma}_r = I_{N_r \times N_r}$ and $\boldsymbol{\Sigma}_t = I_{N_t \times N_t}$: Uncorrelated Rician fading,
- (iv) $K \neq 0$, $\boldsymbol{\Sigma}_r \neq I_{N_r \times N_r}$ and/or $\boldsymbol{\Sigma}_t \neq I_{N_t \times N_t}$: Correlated Rician fading.

2.3. SM Optimal Detection and Uncoded Average Probability of Error

The optimum antenna and index symbols pairs $(u_{\text{ML}}, v_{\text{ML}})$ with maximum likelihood (ML) sense can be expressed as,

$$(u_{\text{ML}}, v_{\text{ML}}) = \operatorname{argmax}_{u,v} f_{\mathbf{Y}}(\mathbf{y} \mid \mathbf{x}, \mathbf{H}) = \operatorname{argmin}_{u,v} D(\mathbf{y}, \mathbf{h}_u X_v) \quad (2.6)$$

where h_u is the u -th column of H for $u = 1, \dots, N_t$ and X_v is the v -th element of the modulation alphabet \mathcal{X} for $v = 1, \dots, M$. $D(y, h_u X_v)$ is the -modified- distance metric between y and $h_u X_v$ and defined as

$$D(\mathbf{y}, \mathbf{h}_u X_v) = \sqrt{\rho} \|\mathbf{h}_u X_v\|^2 - 2\operatorname{Re}\{\mathbf{y}^\dagger \mathbf{h}_u X_v\}. \quad (2.7)$$

In the context of this channel model it is possible to approximate the average SM bit error probability with optimum ML detection using upper bounding technique in [15] as,

$$\begin{aligned} P_b &\leq \mathbb{E}_{\mathbf{x}, \mathbf{H}} \left[\sum_{\hat{u}, \hat{v}} \frac{N(u, \hat{u}, v, \hat{v})}{\log_2(N_t M)} \Pr \{D(\mathbf{y}, \mathbf{h}_u X_v) > D(\mathbf{y}, \mathbf{h}_{\hat{u}} X_{\hat{v}}) \mid \mathbf{h}_u, \mathbf{h}_{\hat{u}}, X_v, X_{\hat{v}}\} \right] \\ &= \frac{1}{N_t M} \sum_{u=1}^{N_t} \sum_{\hat{u}=1}^{N_t} \sum_{v=1}^M \sum_{\hat{v}=1}^M \frac{N(u, \hat{u}, v, \hat{v})}{\log_2(N_t M)} P_s(u, \hat{u}, v, \hat{v}) \end{aligned} \quad (2.8)$$

Where $N(u, \hat{u}, v, \hat{v})$ is number of bits in error between (h_u, X_v) and $(h_{\hat{u}}, X_{\hat{v}})$, the respective channel and symbol pairs. The term $\log_2(N_t M)$ in (2.8) reflects the complete amount of antenna and symbol bits and this term used in division as a summation weight for the respective pairwise error probability (PEP). In the case $\log_2(N_t M) \gg 1$ then the term $\mathbb{E} \left[\frac{N(u, \hat{u}, v, \hat{v})}{\log_2(N_t M)} \right]$ is approximates to 1/2 and (2.8) can be rewritten simply as

$$P_b \leq \frac{1}{2N_t M} \sum_{u=1}^{N_t} \sum_{\hat{u}=1}^{N_t} \sum_{v=1}^M \sum_{\hat{v}=1}^M P_s(u, \hat{u}, v, \hat{v}) \quad (2.9)$$

Similar to [10, 33]. Conditional APEP expression in (2.9) can be derived as,

$$\begin{aligned}
P_s(u, \hat{u}, v, \hat{v}) &= \int_{\mathbf{z}} Q \left(\sqrt{\frac{\|\mathbf{z}\|^2}{2}} \right) f_{\mathbf{z}}(\mathbf{z} \mid \mathbf{h}_u, \mathbf{h}_{\hat{u}}, X_v, X_{\hat{v}}) d\mathbf{z} \\
&= \frac{1}{\pi} \int_0^{\frac{\pi}{2}} \frac{\exp \left(-\tilde{\mathbf{m}}_{\mathbf{z}}^\dagger [\tilde{\Sigma}_{\mathbf{z}} + \sin^2 \theta \mathbf{I}]^{-1} \tilde{\mathbf{m}}_{\mathbf{z}} \right)}{\left| \frac{\tilde{\Sigma}_{\mathbf{z}}}{\sin^2 \theta} + \mathbf{I} \right|} d\theta
\end{aligned} \tag{2.10}$$

And $N_r \times 1$ vector \mathbf{z} defined [6] as,

$$\mathbf{z} = \frac{1}{\sqrt{N_0}} (\mathbf{h}_u X_v - \mathbf{h}_{\hat{u}} X_{\hat{v}}) = \bar{\mathbf{z}} + \tilde{\mathbf{z}} \tag{2.11}$$

Which is by definition [34] a proper complex Gaussian vector. The mean vector and covariance matrix of \mathbf{z} can be expressed as,

$$\mathbf{m}_{\mathbf{z}} = \mathbb{E}[\mathbf{z}] = \sqrt{\frac{K}{N_0(K+1)}} (\bar{\mathbf{h}}_u X_v - \bar{\mathbf{h}}_{\hat{u}} X_{\hat{v}}). \tag{2.12}$$

$$\begin{aligned}
\Sigma_{\mathbf{z}} &= \mathbb{E}[(\mathbf{z} - \mathbf{m}_{\mathbf{z}})(\mathbf{z} - \mathbf{m}_{\mathbf{z}})^\dagger] \\
&= \frac{|X_v|^2 + |X_{\hat{v}}|^2 - 2\text{Re}\{\sigma_{u, \hat{u}}^t X_v X_{\hat{v}}^*\}}{N_0(K+1)} \Sigma_r.
\end{aligned} \tag{2.13}$$

The terms $\tilde{\mathbf{m}}_{\mathbf{z}}$ and $\tilde{\Sigma}_{\mathbf{z}}$ are $\tilde{\mathbf{m}}_{\mathbf{z}} = \frac{\mathbf{m}_{\mathbf{z}}}{2}$ and $\tilde{\Sigma}_{\mathbf{z}} = \frac{\Sigma_{\mathbf{z}}}{4}$ in equation (2.10). Although (2.10) does not simplify further of a closed form expression in cases $m_z \neq 0$, since it is a single definite integral, it can be calculated numerically conveniently for any specified mean vector and covariance matrix. This makes it possible to calculate (2.10) and therefore the right side of (2.8) precisely for any constellation and SM MIMO configuration without resorting to Monte Carlo averaging methods, thereby simplifying the SM error analysis significantly.

2.3.1. Rayleigh Fading

One may notice that further simplification is possible in the Rayleigh fading case, when $K = 0$, $m_z = 0$. Then the covariance matrix becomes,

$$\Sigma_{\mathbf{z}} = \frac{|X_v|^2 + |X_{\hat{v}}|^2 - 2\text{Re}\{\sigma_{u,\hat{v}}^t X_v X_{\hat{v}}^*\}}{N_0} \Sigma_r.$$

Moreover, conditional APEP in (2.10) reduces to;

$$\bar{P}_s^{\text{Rayleigh}}(u, \hat{u}, v, \hat{v}) = \frac{1}{\pi} \int_0^{\frac{\pi}{2}} \left| \frac{\tilde{\Sigma}_{\mathbf{z}}}{\sin^2 \theta} + \mathbf{I} \right|^{-1} d\theta. \quad (2.14)$$

Suppose λ_k for $k = 1, \dots, N_r$ denote the eigenvalues of the matrix $\tilde{\Sigma}_{\mathbf{z}}$. All eigenvalues of $\tilde{\Sigma}_{\mathbf{z}}$ are distinct in the fully correlated Rayleigh fading case. ($m_z = 0$, $\text{rank}[\tilde{\Sigma}_{\mathbf{z}}] = N_r$).

$$\left| \frac{\tilde{\Sigma}_{\mathbf{z}}}{\sin^2 \theta} + \mathbf{I} \right|^{-1} = \prod_{k=1}^{N_r} \left(\frac{\lambda_k}{\sin^2 \theta} + 1 \right)^{-1} = \sum_{k=1}^{N_r} \xi_k \left(\frac{\lambda_k}{\sin^2 \theta} + 1 \right)^{-1} \quad (2.15)$$

where $\xi_k = \prod_{j \neq k} \left(1 - \frac{\lambda_j}{\lambda_k} \right)^{-1}$ is the k -th residual in the partial fraction expression for $k = 1, \dots, N_r$. This result allows the integration and summation order to be changed in (2.10) as,

$$\begin{aligned} \bar{P}_s^{\text{Rayleigh}}(u, \hat{u}, v, \hat{v}) &= \sum_{k=1}^{N_r} \xi_k \frac{1}{\pi} \int_0^{\frac{\pi}{2}} \left(\frac{\lambda_k}{\sin^2 \theta} + 1 \right)^{-1} d\theta \\ &= \frac{1}{2} \sum_{k=1}^{N_r} \xi_k \left(1 - \sqrt{\frac{\lambda_k}{1 + \lambda_k}} \right). \end{aligned} \quad (2.16)$$

Note that (2.16) second line is because of ([35], Appendix B) becomes,

$$\begin{aligned} J_n(c) &= \frac{1}{\pi} \int_0^{\frac{\pi}{2}} \left(\frac{\sin^2 \theta}{\sin^2 \theta + c} \right)^n d\theta \\ &= [P(c)]^n \sum_{k=0}^{n-1} \binom{n-1+k}{k} [1-P(c)]^k \end{aligned} \quad (2.17)$$

where $P(c) = \frac{1}{2} \left(1 - \sqrt{\frac{c}{1+c}} \right)$. In the case of correlation matrix has repeated eigenvalues the partial fraction expansion in (2.15) has terms in the form of $\left(\frac{\lambda_k}{\sin^2 \theta} + 1 \right)^{-t}$ where $t > 1$. In that case the expansion coefficients can be found and the ABEP can still be computed. The extreme case is when there is no receiver correlation, which result in $t = N_r$. In this situation The APEP can be expressed directly as

$$\bar{P}_s^{\text{Rayleigh}}(u, \hat{u}, v, \hat{v}) = J_{N_r}(\bar{\rho}) \quad (2.18)$$

$J_{N_r}(\cdot)$ is defined in (2.17). The value of $\bar{\rho}$ depends on the presence of transmit correlation and the values of X_v and $X_{\hat{v}}$ such that

$$\bar{\rho} = \frac{|X_v|^2 + |X_{\hat{v}}|^2 - 2\text{Re}[\sigma_{u,\hat{u}}^t X_v X_{\hat{v}}^*]}{4N_0}. \quad (2.19)$$

In summary, the APEP, $\bar{P}_s(u, \hat{u}, v, \hat{v})$ can be conveniently calculated in closed form, considering any two pair of the channel and symbol indices. As in the Rician fading case, it is then become straightforward to precisely calculate the ABEP upper bound in (2.8).

3. EQUAL AND UNEQUAL ERROR PROTECTION STRATEGIES

As pointed out in [7], the area of SM is relatively new and even many of the factors affecting the performance of uncoded SM systems are not fully investigated. Therefore, starting from uncoded SM systems with various transmit antennas and present an insight in which conditions an equal error protection is required and in which conditions unequal error protection is necessary. Even if some of the same exact results are presented in the related literature [18], they have not been considered within the framework of error protection schemes for SM. In this chapter observations are made based on uncoded SM antenna and symbol bits error performance comparison.

3.1. Uncoded SM Antenna and Symbol Bits Comparison

To better see the channel effects on antenna and symbol bits, uncoded SM system BER performance is observed with a different approach. Antenna and symbol bits error performances separately simulated over various channel conditions such as uncorrelated Rayleigh/Rician correlated Rayleigh/Rician. The SM system is simulated with 4 transmit and 4 receive antennas and using 16 QAM modulation. The exponential correlation model of [36] is considered where the correlation matrix entries formed as,

$$[\mathbf{\Sigma}]_{u,v} = \sigma_{u,v} = \alpha^{|u-v|}$$

where α is a fixed (real or complex) correlation coefficient between adjacent antennas. In this simulation correlation coefficients α_t and α_r are chosen 0.8, which is used to model strong correlation on transmitter and receiver. In Figure 3.1 simulation results for uncorrelated and correlated Rayleigh fading channel is presented. Although in uncorrelated case antenna and symbol bits error performance is close to each other, antenna bits performance is worse in correlated channel. This apparently shows that antenna bits need more protection in the correlated channel conditions and unique

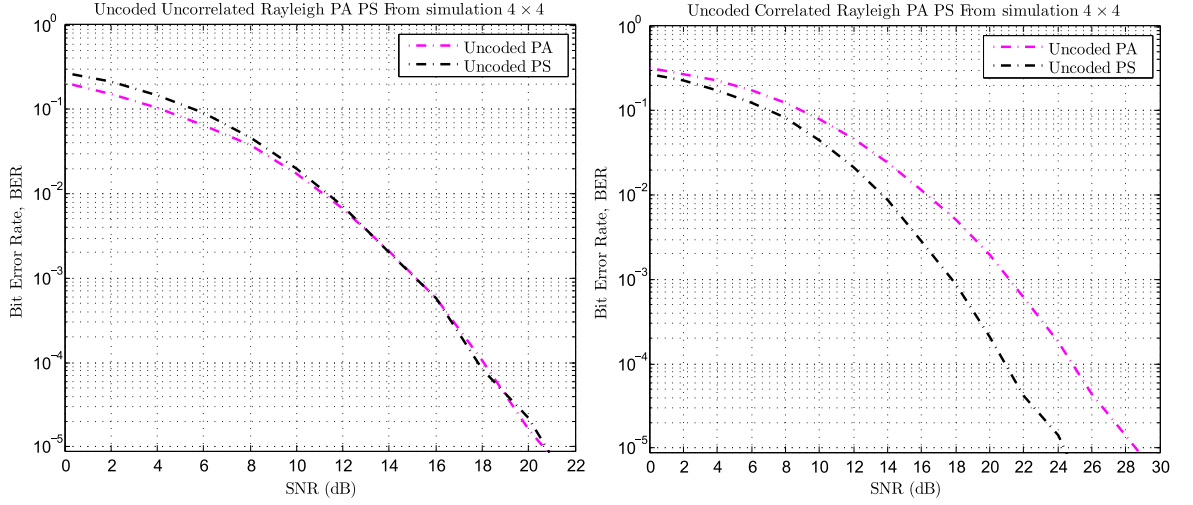


Figure 3.1. Uncoded Antenna and Symbol Bits Performance over Rayleigh Fading Channels.

nature of SM system is very suitable to implement unequal error protection. Specifically for uncorrelated Rayleigh fading case equal error protection is feasible. In Figure 3.2

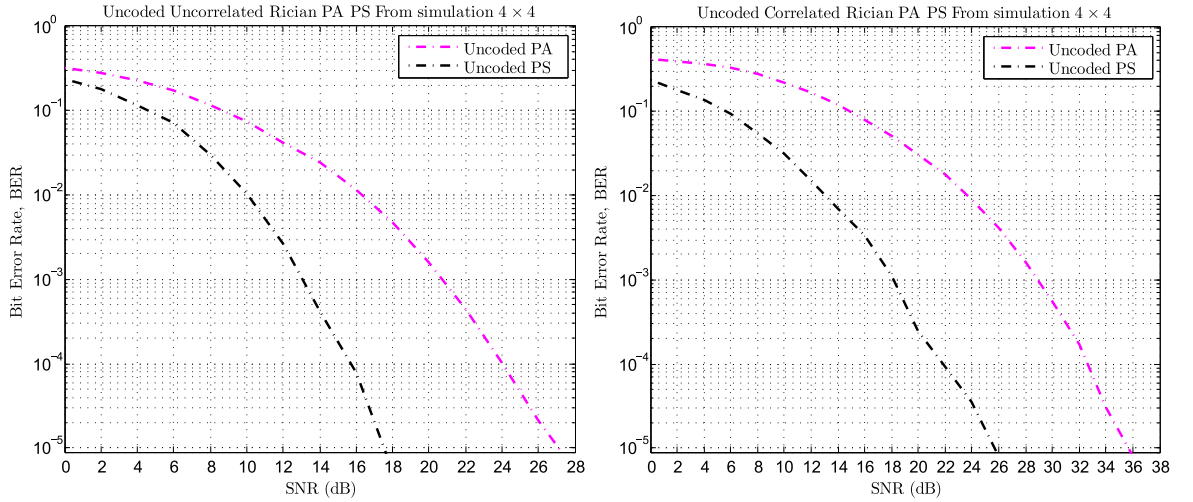


Figure 3.2. Uncoded Antenna and Symbol Bits Performance over Rician Fading Channels.

simulation results for uncorrelated and correlated fading channels is presented with Rician factor $K=3$. One can observe that in uncorrelated Rician fading channel antenna bits error performance is worse than symbol bits error performance. Performance difference at 1×10^{-3} BER level is 3 dB. Even this performance difference is more increased in correlated Rician fading channels as at 1×10^{-2} BER level to 10 dB. Coding strategy for Rician fading channel has to be strongly unequal. Antenna bits need more protection compared to symbol bits. These simulation results are compatible

with the findings of [13]. Although uncoded antenna and symbol bit simulations give an insight of unequal protection in certain channels, it doesn't give an answer to the question of how much unequal protection is required.

3.2. Quantification of Error Protection with New Metric

Quantity of error protection is required for both antenna and symbol bits can be observed with help of a new metric. General ABEP upper bound for uncoded SM is,

$$P_b \leq \frac{1}{N_t M} \sum_{u=1}^{N_t} \sum_{\hat{u}=1}^{N_t} \sum_{v=1}^M \sum_{\hat{v}=1}^M \frac{N(u, \hat{u}, v, \hat{v})}{\log_2(N_t M)} P_s(u, \hat{u}, v, \hat{v}) \quad (3.1)$$

From that point respective ABEP upper bounds for the antenna and symbol bits can be written as,

$$P_b^a \leq \frac{1}{N_t M} \sum_{u=1}^{N_t} \sum_{\hat{u}=1}^{N_t} \sum_{v=1}^M \sum_{\hat{v}=1}^M \frac{N(u, \hat{u})}{\log_2(N_t)} P_s(u, \hat{u}, v, \hat{v}) \quad (3.2)$$

$$P_b^s \leq \frac{1}{N_t M} \sum_{u=1}^{N_t} \sum_{\hat{u}=1}^{N_t} \sum_{v=1}^M \sum_{\hat{v}=1}^M \frac{N(v, \hat{v})}{\log_2(M)} P_s(u, \hat{u}, v, \hat{v}) \quad (3.3)$$

Where $N(u, \hat{u})$ denotes number of different bits between indices of u -th and \hat{u} -th transmit antennas. Similarly, $N(v, \hat{v})$ denotes the number of different bits between the indices of the v -th and \hat{v} -th symbols in the modulation alphabet. Because of being $N(u, \hat{u}, v, \hat{v}) = N(u, \hat{u}) + N(v, \hat{v})$ it is easy to verify that,

$$P_b = \frac{P_b^a}{\log_2(M)} + \frac{P_b^s}{\log_2(N_t)} \quad (3.4)$$

P_b^a and P_b^s can also be obtained using APEP equation (2.10). The ratio of P_b^a/P_b^s can be used as a metric to measure unequal adverse effects of channels such as Rician fading and transmit correlation since P_b^a and P_b^s are expected to be in tight agreement with actual simulated ABEP results at large SNR values. To better observe the channel

effects P_b^a/P_b^s curves for uncoded SM system using 4 transmit and 4 receive antennas is presented. All ABEP bounds are obtained at 24 dB SNR and implementing QPSK modulation.

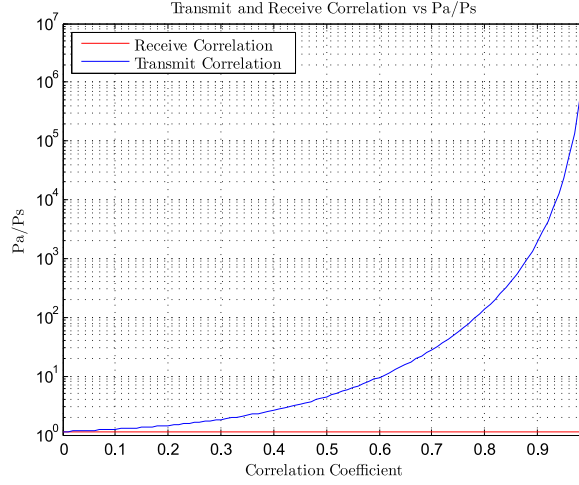


Figure 3.3. Transmit Correlation effects on P_b^a/P_b^s

In Figure 3.3 effects of transmit correlation is observed in Rayleigh fading channel. ($K=0$) For comparison receive antenna correlation is fixed to uncorrelation and only effects of transmit correlation coefficient α_t on P_b^a/P_b^s is observed. The value of $\alpha_t = 0$ and $\alpha_t = 1$ correspond to the completely uncorrelated and completely correlated scenarios respectively. One can observe that in the case of Rayleigh fading channels when there is no transmit correlation the symbol and antenna bit error probability is close to each other. This result is compatible with simulations in previous section and equal error protection is feasible in that condition. On the other hand when the correlation effects increase, antenna bits are more detrimentally affected than symbol bits. As a result of this, P_b^a/P_b^s is increased with the increase of α_t .

In Figure 3.5 P_b^a/P_b^s ratio is observed in the Rician fading channels. In first case K , Rician coefficient is increased while there is no transmit and receive correlation. By the increase of K coefficient P_b^a/P_b^s ratio is also greatly increased. This observation shows if the channel is more Rician, antenna bits are affected more detrimentally even there is no correlation. (Uncorrelated Rician)

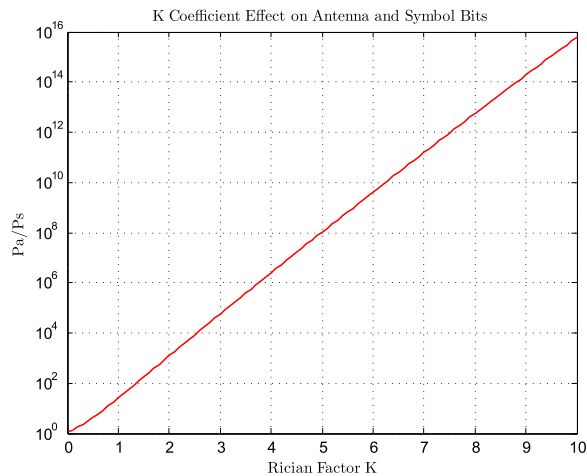
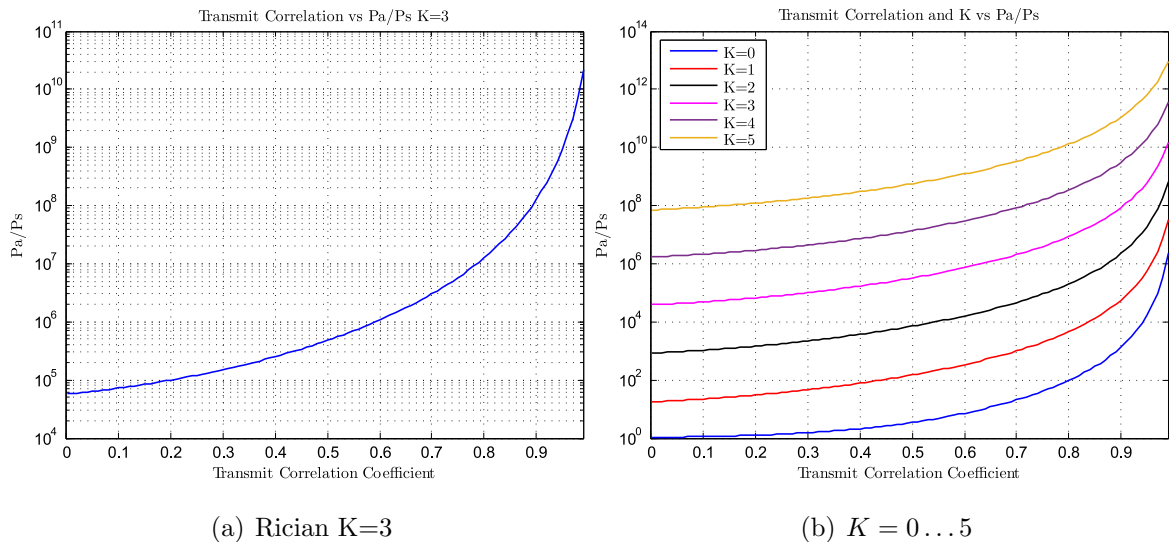


Figure 3.4. Rician coefficient K vs P_b^a/P_b^s



(a) Rician $K=3$

(b) $K = 0 \dots 5$

Figure 3.5. Rician Fading Channels with various K values vs P_b^a/P_b^s .

In Figure 3.5(a) transmit correlation effects on P_b^a/P_b^s is observed for correlated Rician channels. Rician coefficient is assumed to be $K = 3$ and transmit correlation α_t is increased between values $\alpha_t = 0$ to $\alpha_t = 1$. One can notice that, P_b^a/P_b^s is also increasing with the increase of transmit correlation in Rician channels. Hence, the correlated Rician channel is the channel type that most detrimentally affects antenna bits error performance. Another Figure 3.5(b) is also show transmit correlation effects on Rician channels with different Rician coefficients $K = 0, 1, 2, 3, 4, 5$ respectively. As a result the use of unequal error protection strategy is feasible for all Rician channel types.

4. DESIGN AND PERFORMANCE ANALYSIS OF BICSM EEP/UEP

Bit interleaved coded spatial modulation [20] is proposed as an effective technique for not only correct errors due to channel impairments but also as a countermeasure against the presence of Rician fading and spatial correlation. Amount of protection required for antenna and symbol bits in various channel conditions is well described in previous chapter. In this chapter design and method for performance analysis of BICSM system with equal and unequal error protection is presented.

4.1. Equal Error Protection BICSM Design and Performance Analysis

Equal error protection for BICSM is describing the case where antenna and symbol bits are protected by the same effective convolutional code. The system model of BICSM-EEP is shown in Figure 4.1,

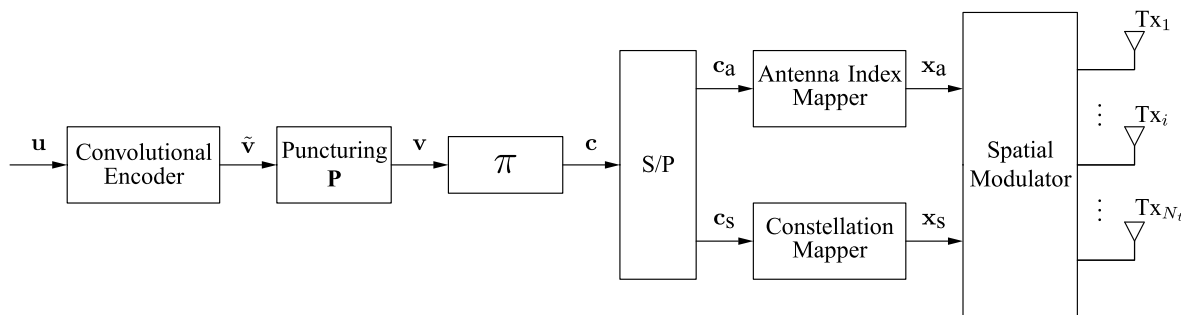


Figure 4.1. Block diagram of BICSM-EEP transmitter system.

The elements of bit sequence \mathbf{u} ($u_i \in \{0, 1\}$, for $i = 1, \dots, L_u$) is processed by a channel encoder to form coded bit sequence \mathbf{v} with elements $v_j \in \{0, 1\}$ for $j = 1, \dots, L_v$. One can notice that block or convolutional codes can be employed in this scheme however because of their use in previous works [18, 19] and flexibility of using puncturing, convolutional codes are considered as a building block of BICSM. Since the punctured codes are key feature of BICSM system the way they are used

and puncture pattern plays important role in overall system performance. The coded sequence is bitwise interleaved by a single bit interleaver to form the sequence with elements c_j for $j = 1, \dots, L_c$. Then interleaver output is demultiplexed into two sets of bits, one for mapping onto antenna indices and other for mapping onto the constellation symbols.

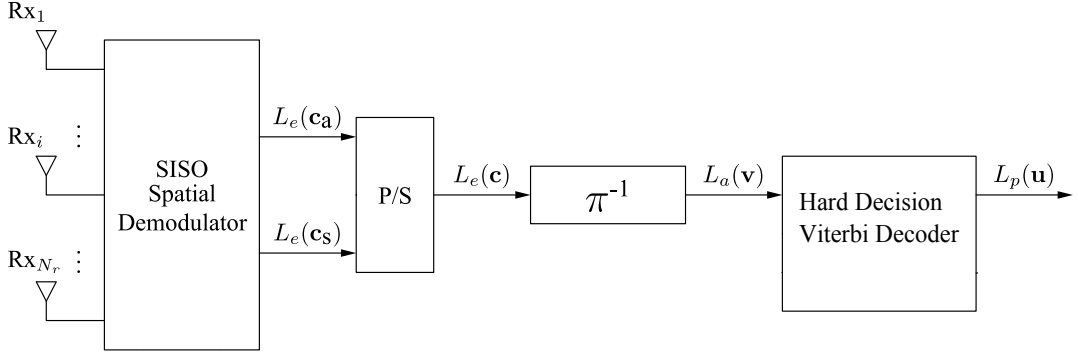


Figure 4.2. Block diagram of BICSM-EEP receiver system.

The receiver shown in Figure 4.2 can use hard decisions and de-map the symbols back to the bits by using mapping alphabet. The antenna and symbol bit sequences (\hat{c}_a , \hat{c}_s) is combined and deinterleaved. Then deinterleaved sequence $L_a(v)$ is decoded by hard decision viterbi decoder. The composite channel between encoder and decoder can be described as a binary symmetric channel (BSC) by assuming infinite interleaving. Corresponding BSC crossover probability is equal to P_b (2.8) uncoded system error probability.

4.2. Upper Bound Derivation for BER Performance of BICSM-EEP

The bit error rate upper bound for the hard decoded BICSM-EEP assuming perfect interleaving can be calculated by method [37],

$$C_{EEP} - ABEP \leq \sum_{d=d_{free}}^{\infty} \frac{1}{k} C_d P_d \quad (4.1)$$

Where d is the Hamming distance, d_{free} is the minimum free distance of the rate k/n convolutional code, C_d is the weighting coefficients and P_d is,

$$P_d = \begin{cases} \sum_{e=\frac{d+1}{2}}^d \binom{d}{e} p^e (1-p)^{d-e} & d \text{ odd} \\ \frac{1}{2} \binom{d}{d/2} p^{d/2} (1-p)^{d/2} + \sum_{e=\frac{d}{2}+1}^d \binom{d}{e} p^e (1-p)^{d-e} & d \text{ even} \end{cases} \quad (4.2)$$

Where p is binary symmetric channel (BSC) transition probability which is ABEP of uncoded SM (2.8) system. For the upper bound calculation weight distribution of convolutional codes (C_d) is a crucial parameter, that reflect coded system behaviour.

4.3. Best Punctured Convolutional Code Search for EEP

The punctured convolutional codes are obtained by periodically perforating coded symbols from the output of a low rate $1/n$ parent code. Punctured convolutional codes have great advantage of flexibility they can be arranged to provide different levels of protection and their decoding is not complex.

Punctured high rate codes are first presented in [38] for rates $R = 2/3, 3/4$ and for low constraint lengths with less complex decoding. Rate $R = (n-1)/n$ codes with low constraint lengths for $n = 2, \dots, 14$ are presented in [39]. Later in studies [40] and [41, 42] puncturing tables are extended to high constraint length codes and also distance spectrums are provided. A more comprehensive study on punctured convolutional codes presented in [43] with optimum distance spectrum weight distributions for AWGN and Rayleigh channels. Although weight distribution of optimum conventional convolutional codes are well tabulated [43, 44] in literature, optimum weight distribution of punctured convolutional codes are not complete for all code rates or are limited to certain channel types.

Binary generator matrix of punctured convolutional codes are expressed as octal integers. Constraint length \bar{K} is defined as the number of memory cells plus one. The

size of puncturing matrix is $n \times p$ where p is puncturing period and the matrix consist of zeros and ones. Puncturing a good rate $1/n$ parent convolutional code also result in good punctured codes. Puncturing patterns positions of perforation has critical importance for code performance. Puncturing a parent convolutional code may result in catastrophic codes or some symmetric and equivalent of other codes. A catastrophic code is described as a convolutional code that finite numbers of channel errors cause infinite number of decoder errors. Catastrophic codes don't provide any error correction for the system.

There is no general algebraic method for designing good convolutional codes. In general a computer search is made based on some criterion such as d_{free} , weight distribution etc. The d_{free} indicate minimum free distance which is the smallest distance between any two code sequences in the code. Design criterion is also depends on where the code is used, the types of channels or system. In literature code search is generally made the criterion based on maximum free distance. Although they are good codes, bit error rate for a coded communication system is not only determined by the free distance of the code. As a better search alternative, performance based search technique is used in this thesis. Thanks to the property of BICSM hard decoding, channel can be modelled as BSC and upper bounding technique in (4.1) can be used for performance comparison of different punctured codes. For EEP the punctured codes with the rates in form $R = n/k, n/(k-1), n/(k-2) \dots$ is in interest. Weight distribution search of punctured convolutional codes of with various rates $R = 4/7, 4/6, 4/5$ employed with IT++ [45], which is C++ library for communication systems. The weight spectrum C_d is calculated in IT++ using breadth first search algorithm. In weight distribution search some perforation patterns result in catastrophic codes. These patterns are discarded from performance evaluation.

Optimum codes for interested coded rates $R = 4/8, 4/7, 4/6, 4/5$ are found by extensive simulation for puncturing period $p = 4$, constraint length $\bar{K} = 3, \bar{K} = 5$ and from parent code with rate $R = 1/2$ convolutional code with generator matrix expressed in octal form (5,7) and (23,35). The puncturing position is indicated by the octal representations of the rows of the puncturing matrix. For in-

stance (5, 17) represent puncturing matrix $\begin{bmatrix} 0 & 1 & 0 & 1 \\ 1 & 1 & 1 & 1 \end{bmatrix}$ and punctured bit position is $\begin{bmatrix} 0, 1, 1, 1, 0, 1, 1, 1 \end{bmatrix}$, 1^{st} and 5^{th} bits.

Performance bounds obtained by using equation (4.1) and comparison is made for channel conditions uncorrelated Rayleigh/Rician and correlated Rayleigh/Rician for BICSM-EEP. In simulations BICSM-EEP system with 4 transmit and 4 receive antennas are employed. As a unique property of BICSM system coded bits mapping to modulation symbols depends on the puncturing implemented. Since there are 4 transmit antennas, in every case $\log_2(N_t) = 2$ bits of coded sequence is mapped to antennas. For one bit puncturing with rate $R = 4/7$ remaining 5 bits are mapped to 32 QAM symbol constellation. Performance bounds for one bit puncturing from rate $R = 1/2$ with (5, 7) generator parent code in Rayleigh and Rician channels are presented in Figures 4.3 and 4.4 as,

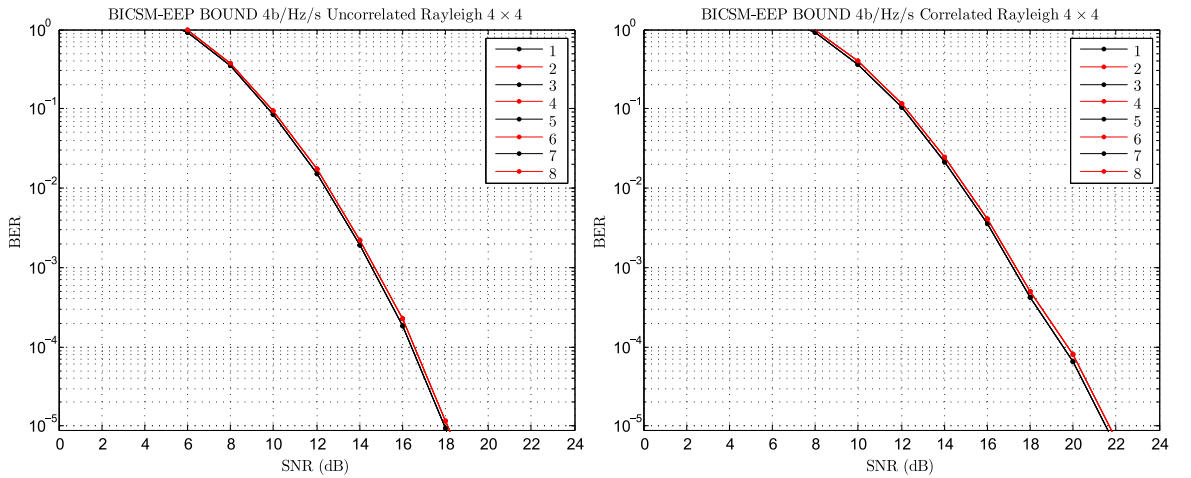


Figure 4.3. EEP scheme BER performance in Rayleigh fading channels with one bit puncturing pattern.

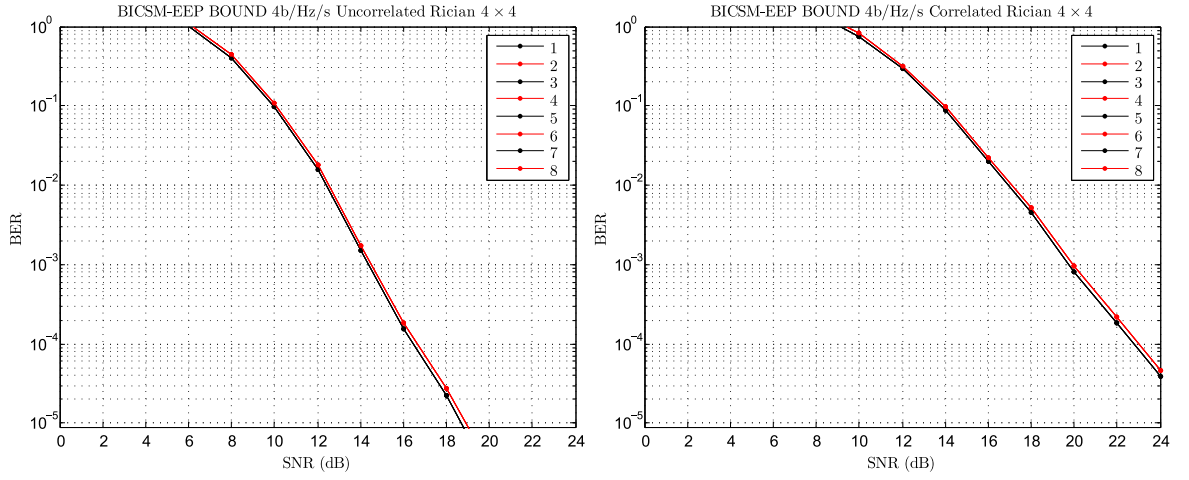


Figure 4.4. EEP scheme BER performance in Rician fading channels with one bit puncturing pattern.

Where black plots represents best codes while blue plots are worst. Punctured bit positions are indicated by the sequence numbers i.e, 4 means 4th bit. For two bit puncturing with rate $R = 4/6$ remaining 4 bits are mapped to 16 QAM symbol constellation. Performance bounds for two bit puncturing from rate $R = 1/2$ with (5, 7) generator parent code in Rayleigh and Rician channels are presented in Figures 4.5 and 4.6 as,

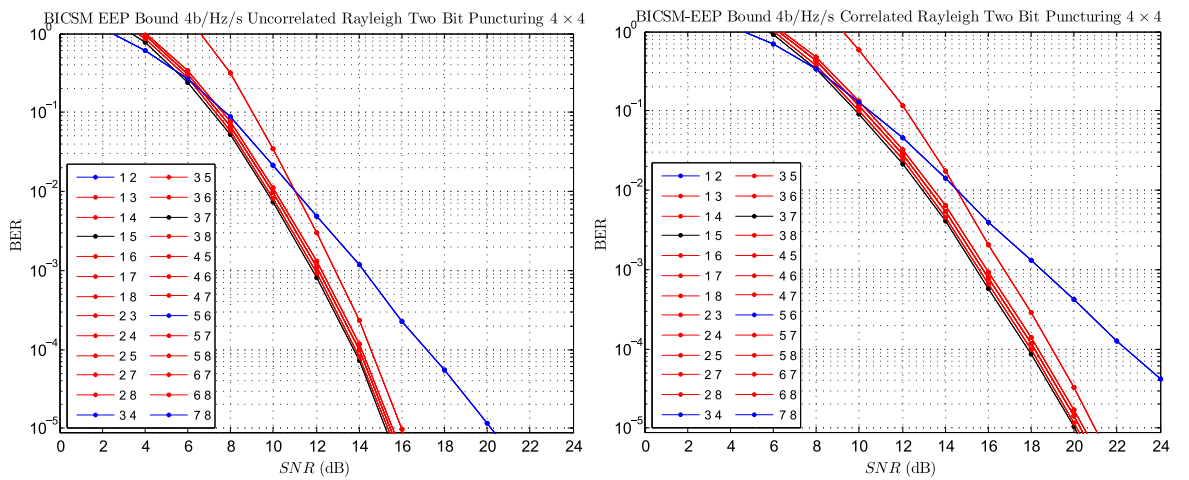


Figure 4.5. EEP scheme BER performance in Rayleigh fading channels with two bits puncturing pattern.

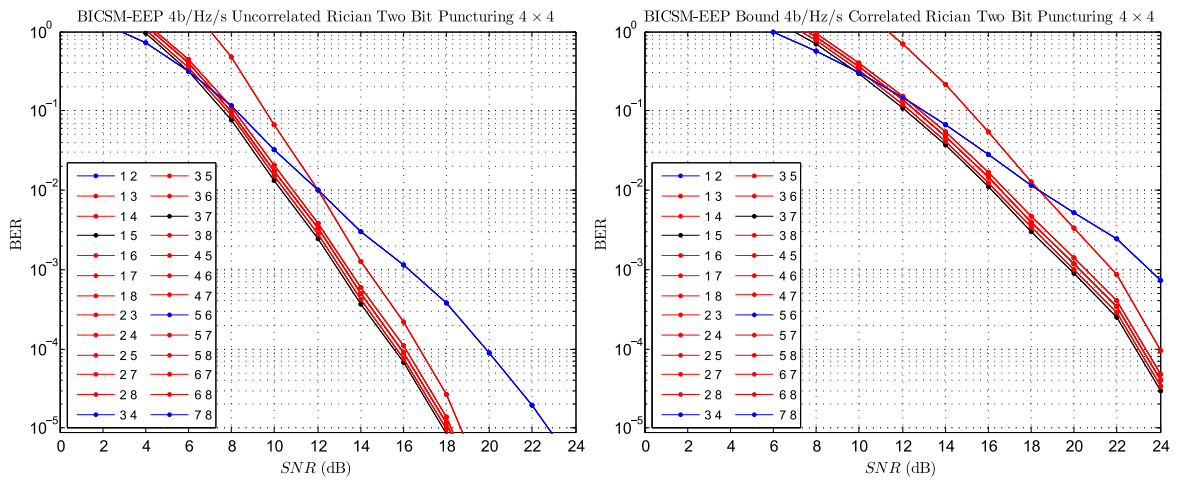


Figure 4.6. EEP scheme BER performance in Rician fading channels with two bits puncturing pattern.

For three bit puncturing with rate $R = 4/5$ remaining 3 bits are mapped to 8 PSK symbol constellation. Performance bounds for three bit puncturing from rate $R = 1/2$ with (5, 7) generator parent code in Rayleigh and Rician channels are presented in Figures 4.7 and 4.8 as,

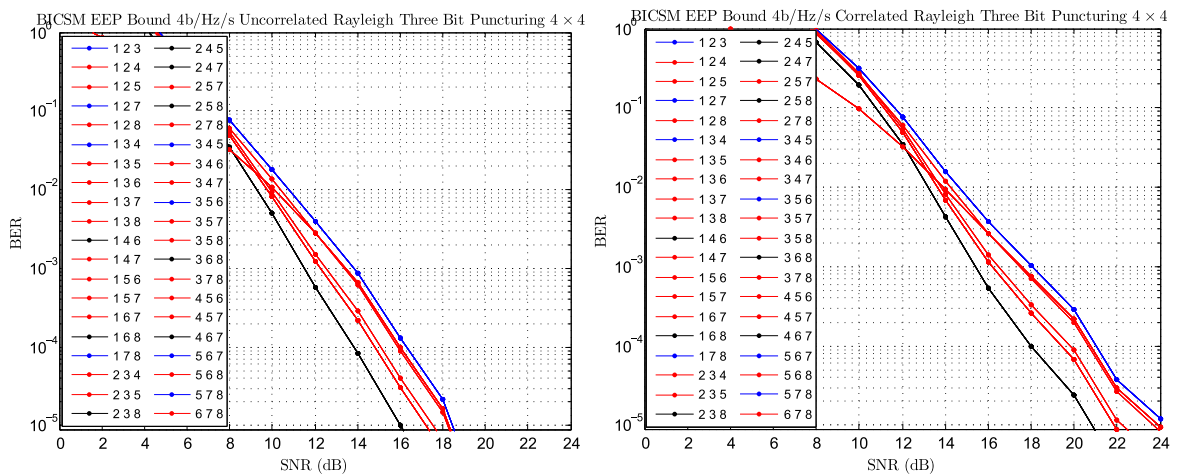


Figure 4.7. EEP scheme BER performance in Rayleigh fading channels with three bits puncturing pattern.

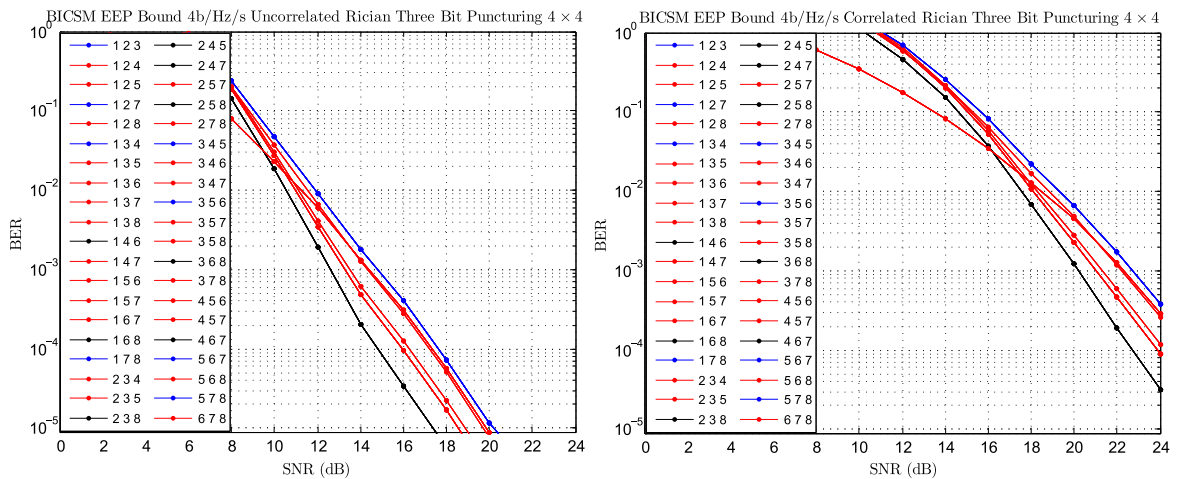


Figure 4.8. EEP scheme BER performance in Rician fading channels with three bits puncturing pattern.

For correlated channels correlation coefficients are calculated with the same exponential method as in Section 3.1 also α_t and α_r are chosen 0.8 to model strong correlation. Best performing codes for all puncturing patterns for rates $R = 4/7, 4/6, 4/5$ and correlated/uncorrelated Rayleigh/Rician channels are obtained by comparison of error performance bounds. Then putting all together and also by employing weight distribution search, optimum punctured codes are tabulated in Table 4.1 as,

Table 4.1. EEP Weight Distribution $n = 2, \bar{K} = 3, p = 4, (5, 7)$

R	$Punct.$	d_f	$[c_d, d = d_f, d_f + 1, \dots, d_f + 6]$
4/8	17, 17	5	4, 16, 48, 128, 320, 768, 1792
4/7	7, 17	4	4, 19, 72, 224, 646, 1794, 4810
4/6	5, 17	3	2, 20, 108, 452, 1706, 6076, 20846
4/5	7, 11	2	1, 36, 309, 2058, 12031, 65754, 344656

Similar comparison is also done for punctured convolutional codes from $(23, 35)_8$ parent code. Optimum punctured codes with corresponding weight distributions are tabulated in Table 4.2 as,

Table 4.2. EEP Weight Distribution $n = 2$, $\bar{K} = 5$, $p = 4$, $(23, 35)$

R	$Punct.$	d_f	$[c_d, d = d_f, d_f + 1, \dots, d_f + 6]$
4/8	17, 17	7	16, 48, 80, 288, 900, 2000, 5296
4/7	7, 17	5	4, 22, 95, 237, 942, 2957, 8809
4/6	7, 13	4	2, 48, 184, 893, 4125, 17255, 73239
4/5	5, 13	3	11, 78, 753, 6890, 51597, 384985, 2729430

4.4. Simulation Results for EEP

In this section simulation results are presented to validate and compare proposed theoretical upper bounds for error performances of BICSM-EEP system under uncorrelated/correlated Rayleigh and uncorrelated/correlated Rician fading channels. Theoretical upper bounds are calculated by using equation (4.1) and bounds are compared with Monte Carlo simulations. For all simulations, BICSM system with 4 transmit and 4 receive antennas are considered.

To better compare BER performance of different BICSM-EEP schemes, spectral efficiency is considered 4 b/s/Hz for all cases and coding rates are chosen accordingly as $R = 4/8, 4/7, 4/6, 4/5$. Modulation alphabet size is chosen compatible with the corresponding coding rates, 64 QAM for $R = 1/2$, 32 QAM for $R = 4/7$, 16 QAM for $4/6$, 8 PSK for $4/5$, respectively. Every 4 bits are encoded and coded sequence is mapped to antenna index and symbol constellations. Since there are 4 antennas at the transmitter $\log_2(4) = 2$ bits are always mapped to antenna index while the rest of coded bits are mapped to the compatible symbol constellations. Channel is implemented with general channel model in Section 2.2, in which Rayleigh and Rician channels can be modelled via appropriate parameter selection. For Rician fading channels Rician coefficient K is chosen 3. The channel correlations are modelled by exponential correlation model in Section 3.1, where transmitter and receiver correlation α_t and α_r both are chosen 0.8 which model strong correlation. Gray mapping is assumed for bit to symbol mappings both in theoretical upper bound calculation and simulated performances. For BICSM-EEP, rate $R = 1/2$ convolutional parent code with $(5, 7)_8$ generator polynomial and the rate $R = 4/7, 4/6, 4/5$ punctured convolutional codes from Table 1 are used.

Decoding of all convolutional codes are done by hard decision Viterbi decoder.

In all figures theoretical upper bounds are plotted with dotted lines while simulation results are plotted with solid lines. All curves are drawn down to at least 1×10^{-5} BER levels. One can observe that theoretical performance curves are in agreement with the simulation results and they are relatively tight especially at high SNR. Additionally, performance curve of uncoded SM system is also provided for better comparison with coded performance improvement. Implemented uncoded SM system is using same number of transmit antenna and QPSK modulation which result in same 4 b/s/Hz spectral efficiency.

Simulation results for 4 b/s/Hz are presented in Figures 4.9 and 4.10 as,

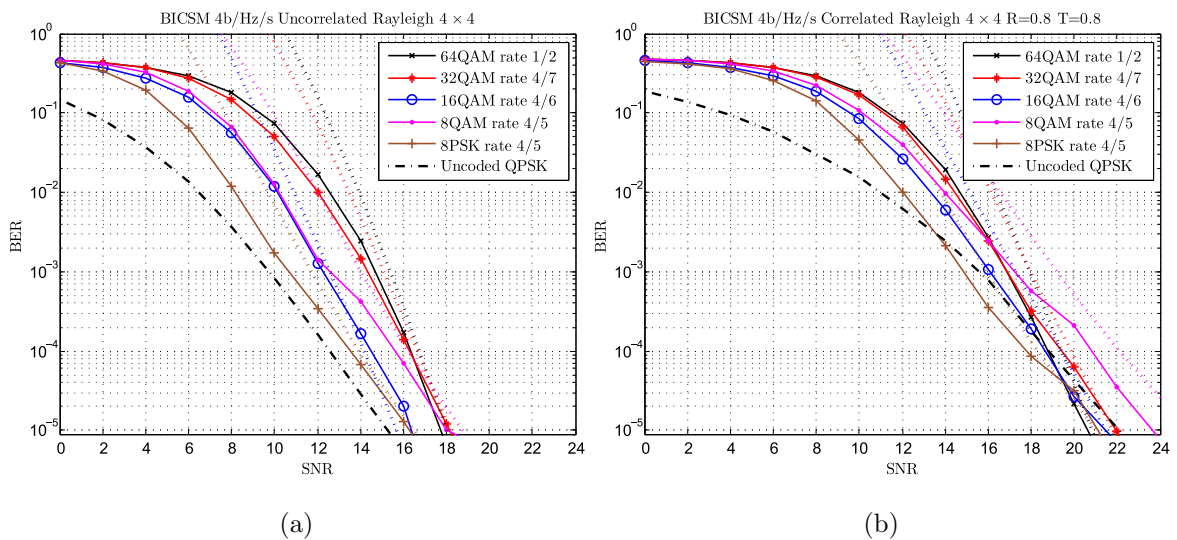


Figure 4.9. EEP scheme performance simulation and upper bound in Rayleigh Fading Channels with various puncturing pattern.

Except the Rayleigh fading case for all cases, the best performance plot is obtained with EEP $R = 1/2$ coding. The error correction capability of punctured convolutional codes are weak compared to parent codes which result in performance degradation. However, in all punctured cases coded bits are mapped to smaller symbol constellations that result in performance improvement since euclidean distance between symbol pairs is increased. Among these two contradicting phenomena performance degradation caused by puncturing overcome the performance improvement caused by increased

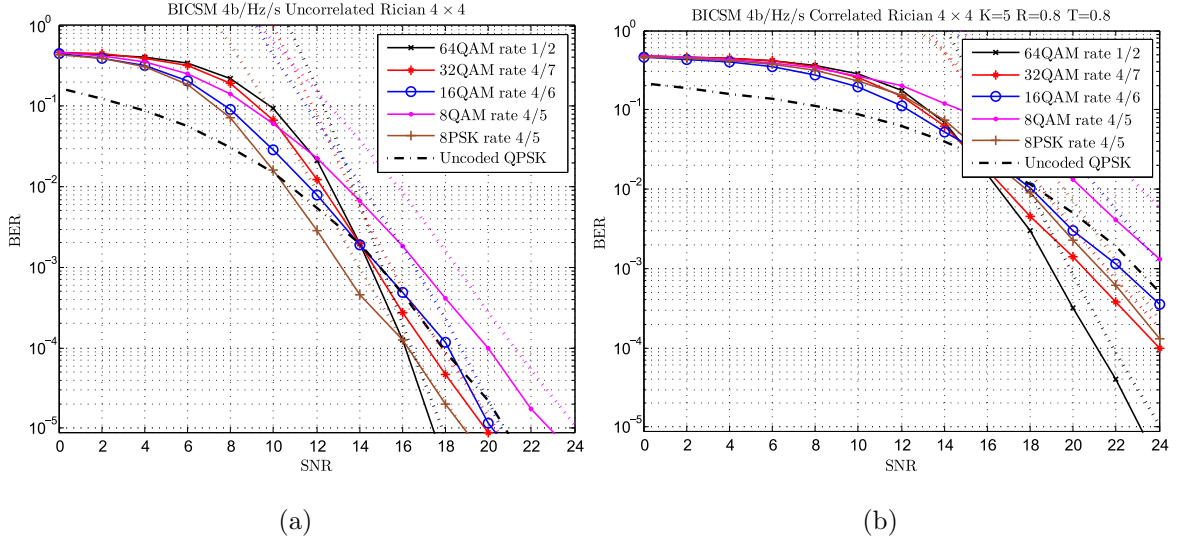


Figure 4.10. EEP scheme performance simulation and upper bound in Rician fading channels with various puncturing pattern.

euclidean distance and overall punctured coded system performance is degraded.

Importance of coding is more obvious in correlated Rician channel. By employing rate 1/2 coded BICSM-EEP 5 dB improvement over uncoded SM can be obtained at 1×10^{-3} BER level.

4.5. Unequal Error Protection BICSM Design and Performance Analysis

Unequal error protection for BICSM is describing the case where antenna and symbol bits are protected by the different rate convolutional codes. The system model of BICSM-UEP is shown in Figure 4.11,

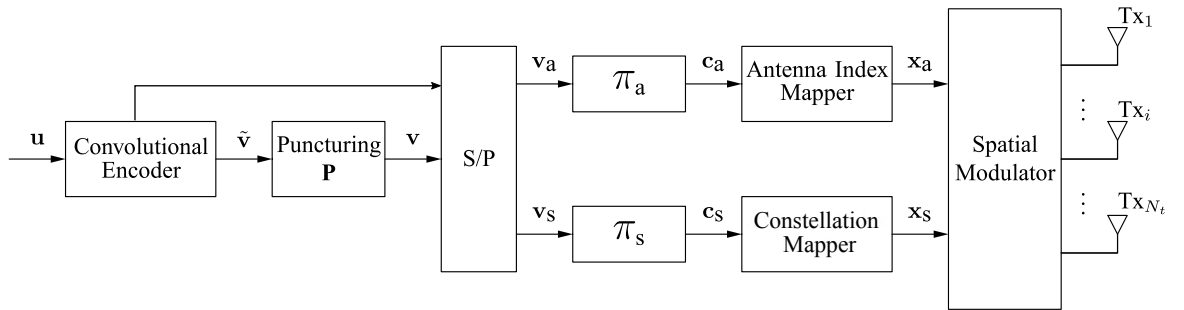


Figure 4.11. Block diagram of BICSM-UEP transmitter system.

The elements of bit sequence u ($u_i \in \{0,1\}$, for $i = 1, \dots, L_u$) is processed by a channel encoder to form coded bit sequence v with elements $v_j \in \{0,1\}$ for $j = 1, \dots, L_v$. One can observe that in BICSM-UEP system, convolutional codes with two different rates are employed to provide different levels of protection for antenna and symbol bits. Because of their implementation flexibility punctured convolutional codes are also chosen for this scheme. While antenna bits are protected with parent convolutional code, symbol bits are protected with various rate punctured convolutional codes. The coded sequence is bitwise interleaved to form the sequence with elements c_j for $j = 1, \dots, L_c$. Then interleaver outputs are mapped to respective antenna indices and symbol constellations.

The BICSM-UEP receiver scheme is depicted in Figure 4.12,

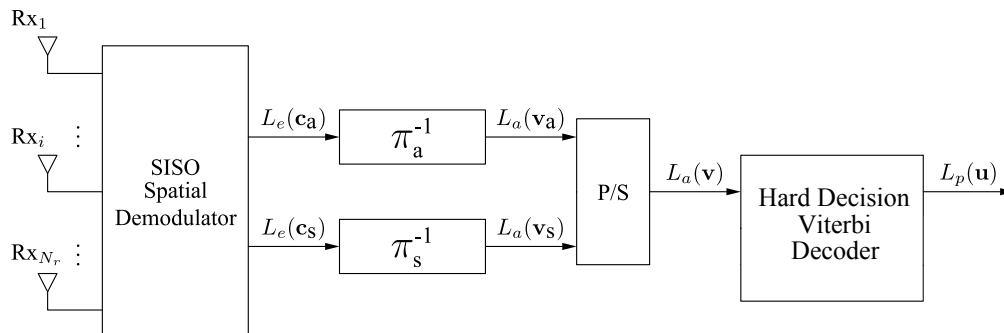


Figure 4.12. Block diagram of BICSM-UEP receiver system.

The receiver shown in Figure 4.12 firstly de-map the symbols back to the bit stream by using mapping alphabet. The antenna and symbol bit sequences deinterleaved respectively. Deinterleaved coded sequence $L_a(v)$ is then decoded by hard decision viterbi decoder. As in the EEP case, the composite channel between encoder and decoder can be described as two parallel BSC by assuming infinite interleaving. Corresponding BSC crossover probability is different from EEP case since there is different levels of contributions from uncoded error performances of antenna and symbol bits.

4.6. Upper Bound Derivation for BER Performance of BICSM-UEP

The bit error rate upper bound for the hard decoded BICSM-UEP assuming perfect interleaving can be calculated with the help of separate weighted upper bounds of coded antenna and symbol bits. The upper bound for coded antenna bit error probability is given as,

$$P_c^a \leq \sum_{d=d_{free}}^{\infty} \frac{1}{k} C_d P_d^a \quad (4.3)$$

Where d is Hamming distance, d_{free} is the minimum free distance of the rate k/n convolutional code C_d is weighting coefficients of respective code and P_d^a is,

$$P_d^a = \begin{cases} \sum_{e=\frac{d+1}{2}}^d \binom{d}{e} p^e (1-p)^{d-e} & d \text{ odd} \\ \frac{1}{2} \binom{d}{d/2} p^{d/2} (1-p)^{d/2} + \sum_{e=\frac{d}{2}+1}^d \binom{d}{e} p^e (1-p)^{d-e} & d \text{ even} \end{cases} \quad (4.4)$$

Where p is binary symmetric channel transition probability which is ABEP of uncoded antenna bits. The error probability of uncoded antenna bits P_b^a can be upper bounded as,

$$P_b^a \leq \frac{1}{N_t M} \sum_{u=1}^{N_t} \sum_{\hat{u}=1}^{N_t} \sum_{v=1}^M \sum_{\hat{v}=1}^M \frac{N(u, \hat{u})}{\log_2(N_t)} P_s(u, \hat{u}, v, \hat{v}) \quad (4.5)$$

Upper bound for coded symbol bit error probability is given as,

$$P_c^s \leq \sum_{d=d_{free}}^{\infty} \frac{1}{k} C_d P_d^s \quad (4.6)$$

Where d is Hamming distance, d_{free} is the minimum free distance of the rate k/n convolutional code C_d is weighting coefficients of respective code and P_d^s is,

$$P_d^s = \begin{cases} \sum_{e=\frac{d+1}{2}}^d \binom{d}{e} p^e (1-p)^{d-e} & d \text{ odd} \\ \frac{1}{2} \binom{d}{d/2} p^{d/2} (1-p)^{d/2} + \sum_{e=\frac{d}{2}+1}^d \binom{d}{e} p^e (1-p)^{d-e} & d \text{ even} \end{cases} \quad (4.7)$$

Where p is binary symmetric channel transition probability which is ABEP of uncoded symbol bits. The error probability of uncoded symbol bits P_b^s can be upper bounded as,

$$P_b^s \leq \frac{1}{N_t M} \sum_{u=1}^{N_t} \sum_{\hat{u}=1}^{N_t} \sum_{v=1}^M \sum_{\hat{v}=1}^M \frac{N(v, \hat{v})}{\log_2(M)} P_s(u, \hat{u}, v, \hat{v}) \quad (4.8)$$

By combining and weighting coded antenna and symbol bit error probabilities P_c^a and P_c^s upper bound for overall BICSM-UEP error probability can be expressed as,

$$C_{UEP} - ABEP \leq \frac{\log_2(N_t) P_c^a + \log_2(M) P_c^s}{\log_2(N_t M)} \quad (4.9)$$

4.7. Best Punctured Convolutional Code Search for UEP

Punctured convolutional codes are also key component for design of BICSM-UEP system. In the proposed BICSM-UEP system, the rate $R = 1/2$ convolutional code is employed to protect antenna bits while rate $R = 3/5, 3/4$ punctured convolutional codes are employed to protect symbol bits. The selection of optimum punctured convolutional codes are done with a similar performance based technique used for BICSM-EEP code selection.

By using property of BICSM-UEP hard decoding where the channel can be modelled as two parallel BSC, upper bounding technique in (4.9) can be used for performance comparison of various punctured codes. Weight distribution search of conventional and punctured convolutional codes with rates $R = 3/6, 3/5, 3/4$ are also employed with IT++ [45], C++ communications systems library. In weight distribution search some perforation patterns result in catastrophic codes and these are discarded from performance evaluation.

Optimum punctured codes for interested code rates $R = 3/5, 3/4$ are found via extensive simulation for puncturing period $p=3$, constraint length $\bar{K} = 3, \bar{K} = 5$ and they obtained from rate $R = 1/2$ parent convolutional code with generator matrix expressed in octal form $(5, 7)_8$ and $(23, 35)_8$. The puncturing position is indicated by the octal representation of the puncturing matrix. For instance $(3, 7)_8$ represent puncturing matrix $\begin{bmatrix} 1 & 1 & 0 \\ 1 & 1 & 1 \end{bmatrix}$ and punctured bit position is $[1, 1, 1, 1, 0, 1]$, 5^{th} bit.

Performance bounds are obtained by using equation (4.9) and comparison is made for uncorrelated Rayleigh/Rician and correlated Rayleigh/Rician channel conditions. In all simulations, BICSM-UEP system is implemented with 4 transmit and 4 receive antennas. For every case, incoming 1 bit out of 4 bits is encoded with $R = 1/2$ encoder and the coded 2 bits are mapped to antenna indexes. The rest of incoming 3 bits are encoded separately with rate $R = 3/5$ punctured convolutional code. The coded 5 bits are mapped to 32 QAM symbol constellation. Performance bounds for punctured convolutional coded scheme obtained by one bit puncturing from rate $R = 1/2$ parent code with generator $(5, 7)_8$ in Rayleigh and Rician channels are presented in Figures 4.13 and 4.14 as,

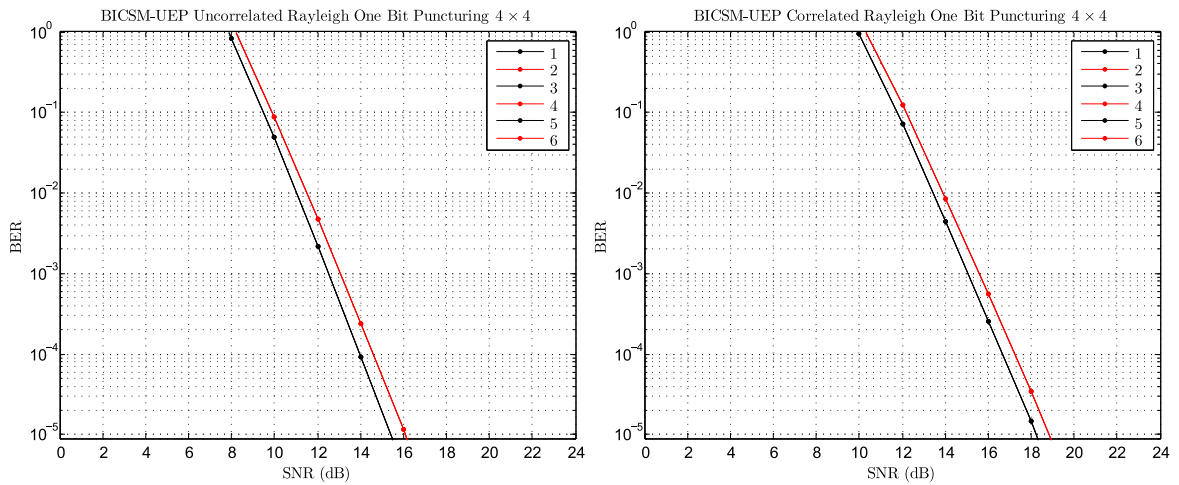


Figure 4.13. UEP scheme in Rayleigh fading channels with one bit puncturing.

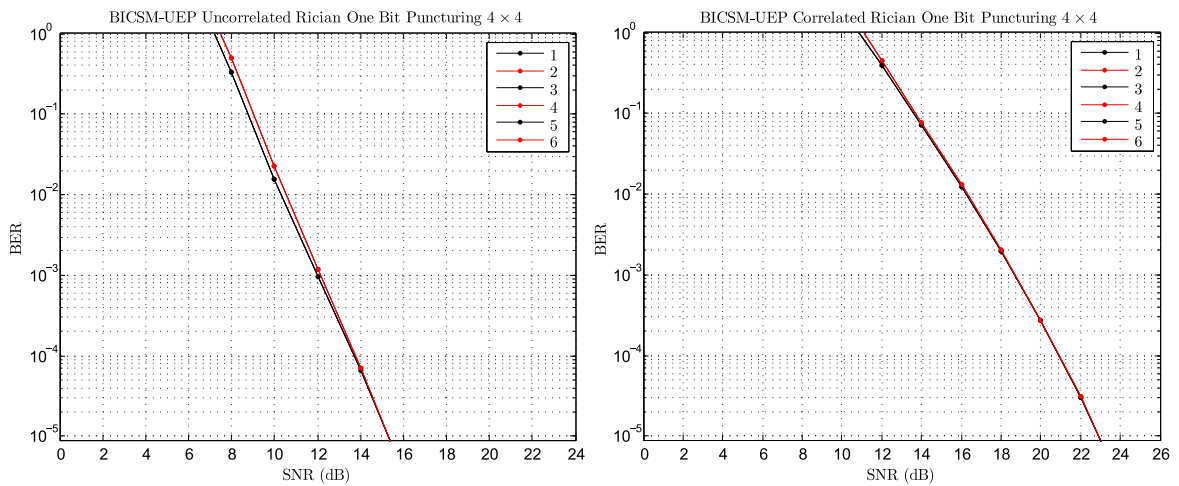


Figure 4.14. UEP scheme in Rician fading channels with one bit puncturing.

Where black plots represents best codes. Punctured bit positions are indicated by sequence numbers. In case of two bit puncturing with rate $R = 3/4$ punctured code, coded 4 bits are mapped to 16 QAM symbol constellation. Performance bounds for two bit puncturing obtained from rate $R = 1/2$ generator $(5, 7)_8$ parent code in Rayleigh and Rician fading channels presented in Figures 4.15 and 4.16 as,

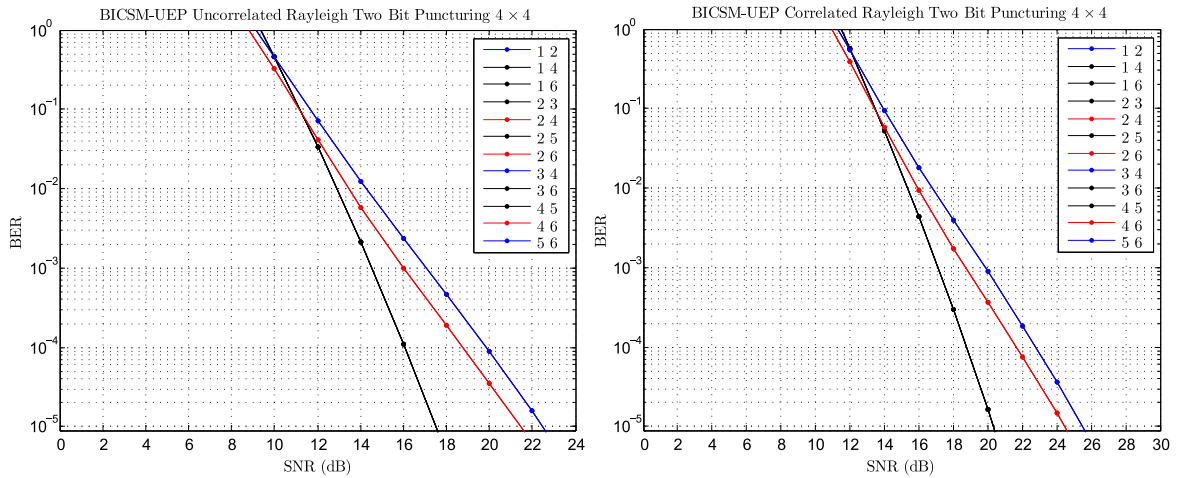


Figure 4.15. UEP scheme in Rayleigh fading channels in two bits puncturing pattern.

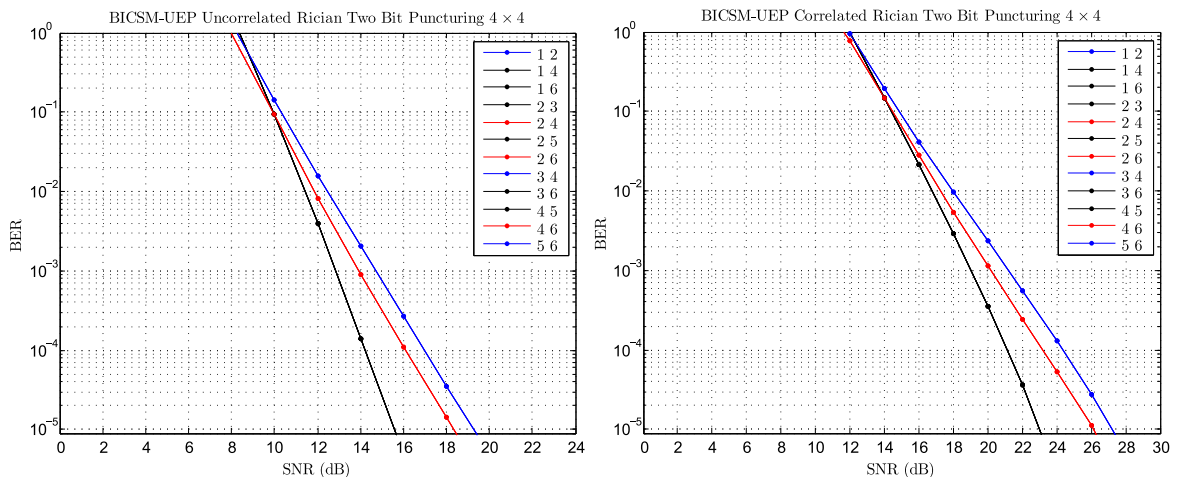


Figure 4.16. UEP scheme in Rician fading channel with two bits puncturing pattern.

Where black plots represents best codes while blue plots are worst. For correlated channels correlation coefficients are calculated with the same exponential method as in Section 3.1 also α_t and α_r are chosen 0.8 to model strong correlation. Best performing codes for all puncturing patterns for rates $R = 3/5$, $3/4$ and correlated/uncorrelated Rayleigh/Rician channels are obtained by comparison of bit error performance bounds. Optimum codes for three different UEP system is tabulated in Table 4.3. While antenna bits are always protected with rate $R = 1/2$ convolutional code symbol bits are protected with various punctured codes and even left uncoded to provide UEP. Optimum punctured codes obtained from parent code with $(5, 7)_8$ generator presented with their weight distributions.

Table 4.3. UEP Weight Distribution $n = 2$, $\bar{K} = 3$, $p = 3$, $(5, 7)$

R	$Punct.$	d_f	$[c_d, d = d_f, d_f + 1, \dots, d_f + 6]$
1/2	–	5	1, 4, 12, 32, 80, 192, 448
3/5	3, 7	4	4, 32, 104, 312, 956, 2792, 7824
1/2	–	5	1, 4, 12, 32, 80, 192, 448
3/4	3, 5	3	15, 104, 540, 2520, 11048, 46516, 190448
1/2	–	5	1, 4, 12, 32, 80, 192, 448
<i>Uncoded</i>	–	–	–

Similar comparison is also done for punctured convolutional codes obtained from $(23, 35)_8$ parent code. Optimum punctured codes with corresponding weight distributions are tabulated in Table 4.4 as,

Table 4.4. UEP Weight Distribution $n = 2$, $\bar{K} = 5$, $p = 3$, $(23, 35)$

R	$Punct.$	d_f	$[c_d, d = d_f, d_f + 1, \dots, d_f + 6]$
3/6	7, 7	7	12, 36, 60, 216, 675, 1500, 3972
3/5	7, 3	5	1, 39, 104, 426, 1556, 5212, 17887
3/4	3, 5	3	1, 7, 125, 936, 5915, 36580, 216612

4.8. Comparative Performance Analysis of BICSM-EEP and BICSM-UEP Systems

In this section various code rates of BICSM-EEP and BICSM-UEP schemes are provided with upper bound simulation results showing how each scheme behaves in uncorrelated Rayleigh/Rician and correlated Rayleigh/Rician channel conditions. This comparative study is not only present the best coding strategy for each channel type but also gives an insight of underlying design criterions.

For all simulations SM system with 4 transmit and 4 receive antennas is considered. The overall system spectral efficiency is fixed to 4 b/s/Hz in UEP and EEP to better compare BER performances. All curves are obtained by using error analysis frameworks proposed in Sections 4.2 for EEP and 4.6 for UEP with the equations 4.1 for EEP and 4.9 for UEP upper bounds.

For each case every 4 bits are encoded and coded bits are mapped to antenna indexes and symbol constellations. Gray mapping is assumed for bit to symbol mappings. In BICSM-EEP system modulation size is chosen with the corresponding coding rates 64 QAM for $R = 1/2$, 32 QAM for $R = 4/7$, 16 QAM for $R = 4/6$, 8 PSK for $R = 4/5$ respectively. In BICSM-UEP system antenna and symbol bits are encoded separately and antenna bits are always encoded with rate $R = 1/2$ convolutional encoder. Symbol bits coding rate and corresponding modulation alphabet size is 32 QAM for $R = 3/5$, 16 QAM for $R = 3/4$ and 8 PSK-QAM for uncoded symbol case. In uncoded symbol case, incoming three bits are directly mapped to 8 PSK or QAM constellation without encoding. Channel is modelled by the general channel model in Section 2.2, where Rayleigh and Rician channels can be modelled with appropriate parameter selection. For all Rician channels Rician coefficient K is chosen 3. The channel correlations are modelled by exponential correlation model in Section 3.1, where transmitter and receiver correlations chosen to model strong correlation with $\alpha_t = 0.8$ and $\alpha_r = 0.8$ respectively. For both BICSM-EEP and BICSM-UEP systems rate $R = 1/2$ convolutional code with $(5, 7)_8$ generator is used to obtain punctured codes. All codes used in BICSM-EEP and BICSM-UEP systems are chosen optimum codes and their weight distributions for upper bound calculations acquired from Table 4.1 and Table 4.3, respectively. Decoding of all convolutional codes are done by hard decision viterbi decoder.

Additionally, performance curve of uncoded SM system is also provided to compare with coded performance improvement. Uncoded scheme is employing 4 transmit antenna and QPSK modulation to achieve 4 b/s/Hz spectral efficiency. All curves are drawn down to at least 1×10^{-5} BER levels.

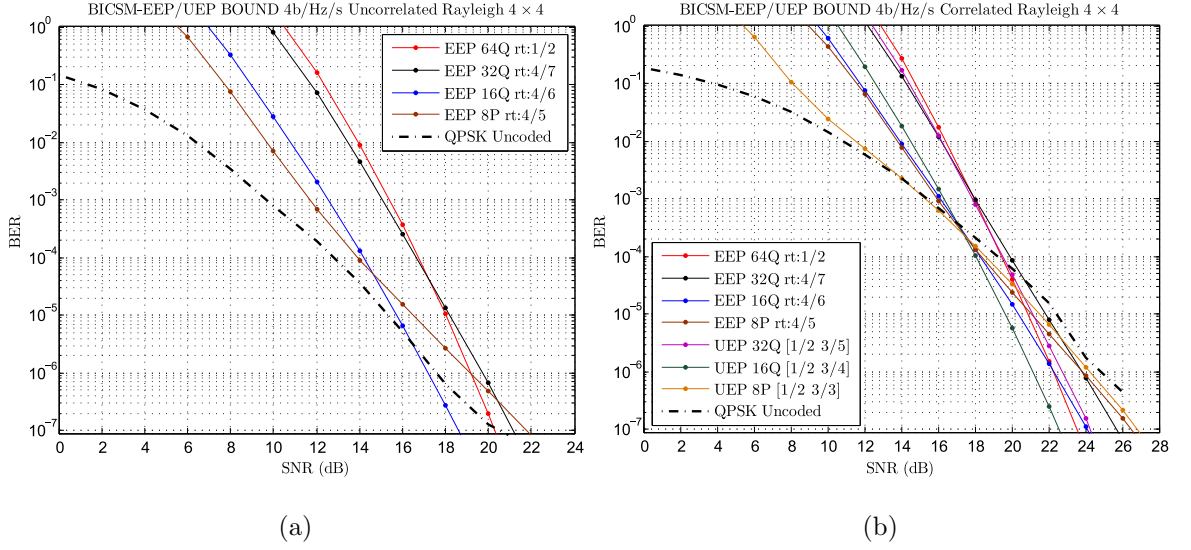


Figure 4.17. EEP/UEP BER performances in uncorrelated/correlated Rayleigh fading channels with various puncturing patterns.

As plotted in Figure 4.17(a) only EEP coding schemes compared in uncorrelated Rayleigh channel with the insight provided in Chapter 3 that antenna and symbol bits are similarly affected by the channel impairments. Among the different coding rates implemented with EEP scheme, optimum two bit punctured coded plot with rate $R = 4/6$ and 16 QAM modulation perform best. At 1×10^{-7} BER level rate $R = 4/6$ code is performing more than 2 dB better than scheme implemented with rate $R = 1/2$ parent code. Although punctured convolutional codes have weak error protection capability compared to conventional convolutional codes this performance improvement can be explained by reduced symbol constellation size. While BICSM-EEP scheme with $R = 1/2$ code employs 64 QAM symbol constellation, the rate $R = 4/6$ code employs 16 QAM. Smaller symbol constellation size result in longer euclidean distance between symbol pairs and this improves performance. Same effect is also can be observed in EEP scheme with rate $R = 4/7$ employing 32 QAM with less amount. Interestingly EEP scheme with rate $R = 4/5$ code employing 8 PSK has worst performance. Since the code is obtained by three bit puncturing, performance loss caused by the puncturing is greater than the performance improvement caused by longer euclidean distance between symbol constellation pairs.

In Figure 4.17(b) performance curves for EEP and UEP schemes are plotted for correlated Rayleigh channel. Antenna and symbol bits affected by channel impairments differently in correlated channels as shown in Chapter 3 where antenna bits are more detrimentally affected. As one can observe UEP scheme implemented with rates $R = [1/2 \ 3/4]$ and 16 QAM symbol constellation is best performing scheme in correlated Rayleigh channel. This result is expected since unequal protection is suitable design strategy for the channels inherently unequal like correlated channels. While antenna bits are protected by strong rate $R = 1/2$ convolutional code, symbol bits are protected with rate $R = 3/4$ two bits punctured code. Despite puncturing, this scheme still performing best because of reduced symbol constellation size which result in greater euclidean distance. Similar UEP scheme implemented with $R = [1/2 \ 3/5]$ and 32 QAM performs 2 dB worse than UEP $R = [1/2 \ 3/4]$ at 1×10^{-7} BER level. This performance decrease caused by larger 32 QAM constellation size and smaller euclidean distance.

Second good performing scheme is EEP rate $R = 1/2$ with 64 QAM as a result of strong protection capability of rate $R = 1/2$ code. There is approximately 1 dB performance difference between these UEP and EEP schemes at 1×10^{-7} BER level. Third and fourth good performing schemes are EEP rate $R = 4/6$ with 16 QAM and UEP rate $R = [1/2 \ 3/5]$ with 32 QAM and their performance is very close to each other at high SNR. Worst performing scheme among all is UEP implemented with $[1/2 \ \text{Uncoded}]$ with 8 PSK constellation. In this scheme while antenna bits are protected with rate $R = 1/2$ code symbol bits are left unprotected. Performance degradation of symbol bits surpassed greatly performance improvements of antenna bits. Overall performance is greatly reduced compared to other coding schemes. Still, even this scheme has performance gain over completely uncoded QPSK scheme. That also shows importance of protecting antenna bits.

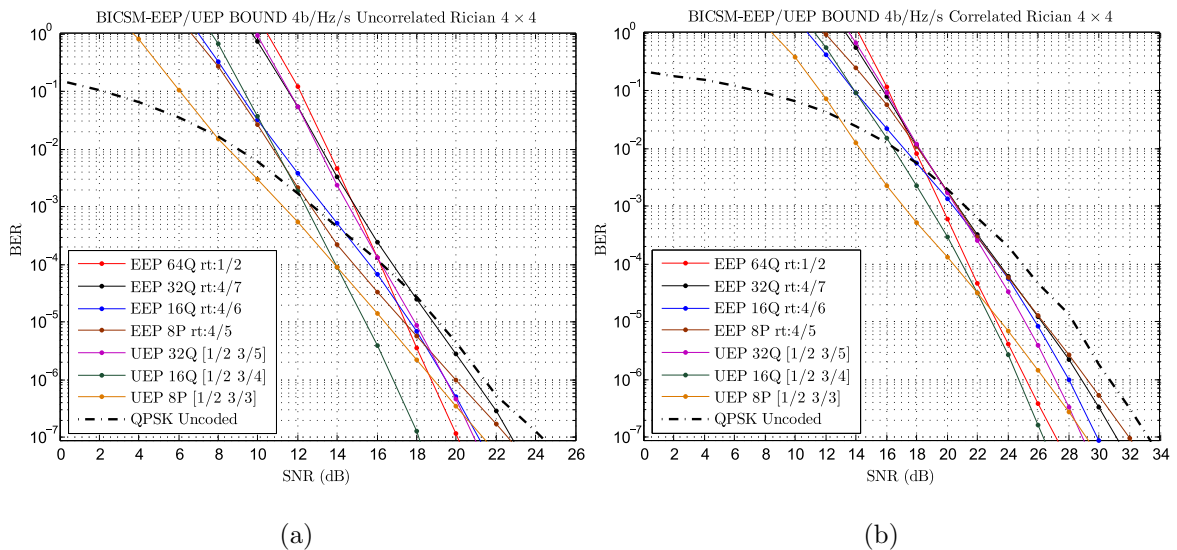


Figure 4.18. EEP/UEP BER performances in uncorrelated/correlated Rician fading channels with various puncturing patterns.

BICSM-EEP/UEP performance curves for various coding schemes shown in Figure 4.18(a) and Figure 4.18(b) respectively. The channel impairments of Rician channels, especially the correlated case affect antenna and symbol bits highly unequal. UEP system with $R = [1/2 \ 3/4]$ and 16 QAM is the best performing scheme for both of these channel types. This result is also expected. Since antenna bits are more detrimentally affected by channel they are protected with rate $R = 1/2$ strong convolutional code and also there is performance gain coming from reduced symbol constellation size. Second good performing scheme for Rician channels is EEP scheme employed with rate $R = 1/2$ code with 64 QAM. This scheme uses advantage of strong rate $R = 1/2$ convolutional code. The reason of this EEP scheme performs worse than UEP scheme can be explained as, its symbol constellation size is 64 QAM with smaller euclidean distance while UEP scheme employs 16 QAM with greater euclidean distance between symbol pairs. There is 2 dB performance difference between UEP $R = [1/2 \ 3/4]$ 16 QAM and EEP $R = 1/2$ 64 QAM at 1×10^{-7} BER level in uncorrelated Rician channel. However performance difference is smaller in the correlated Rician channel, less than 1 dB at 1×10^{-5} BER level. Another observation can be made on performance improvement over uncoded case. Error protection, in the form of UEP or EEP increase BER performance greatly compared to uncoded case. Performance improvement of 6

dB is obtained with the best UEP $R = [1/2 \quad 3/4]$ 16 QAM at 1×10^{-7} BER level over uncoded SM system QPSK. EEP scheme with rate $R = 1/2$ and 64 QAM is performing 4 dB better than uncoded SM system with QPSK at the same BER level.

Important observations can be made based on the plots. Well designed BICSM-UEP system performance can overcome other BICSM schemes in correlated and Rician channels. For uncorrelated Rayleigh channel EEP is the best strategy. BICSM-UEP has design flexibility as seen in plots error protection for symbol bits can be adjusted with the need. One other advantage of UEP scheme is, reduced symbol constellation size, larger euclidean distance and that result in performance improvement.

5. SOFT DECISION DECODING

5.1. Soft Decision Decoding System Model

In this chapter BICSM-EEP/UEP system is implemented with soft input soft output receiver to further improve BER performance. SISO receiver block diagram is shown in Figures 5.1 and 5.2, where the receiver is implemented with SISO SM demodulator followed by a SISO channel decoder. LLRs from demodulator is processed by the SISO channel decoder to form extrinsic LLRs on both the information bits and coded bits. The code LLRs are sent back to the SM demodulator when the receiver employs iterative demodulation/decoding.

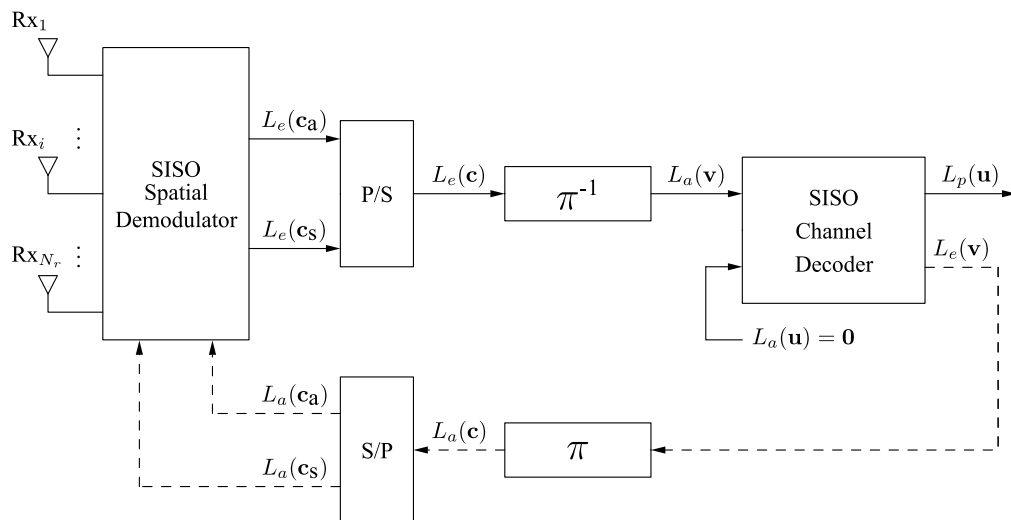


Figure 5.1. Block diagram of SISO BICSM-EEP receiver system.

As pointed in [15] antenna index subsets can be denoted with $\mathcal{U}_{i,1}$ and $\mathcal{U}_{i,0}$ where each element is mapped by n bit codewords whose i -th bit is 1 and 0 respectively. And also symbol index subsets can be denoted with $\mathcal{V}_{i,1}$ and $\mathcal{V}_{i,0}$ where each element is mapped by n -bit codewords whose i -th bit 1 and 0 respectively. LLRs can be computed

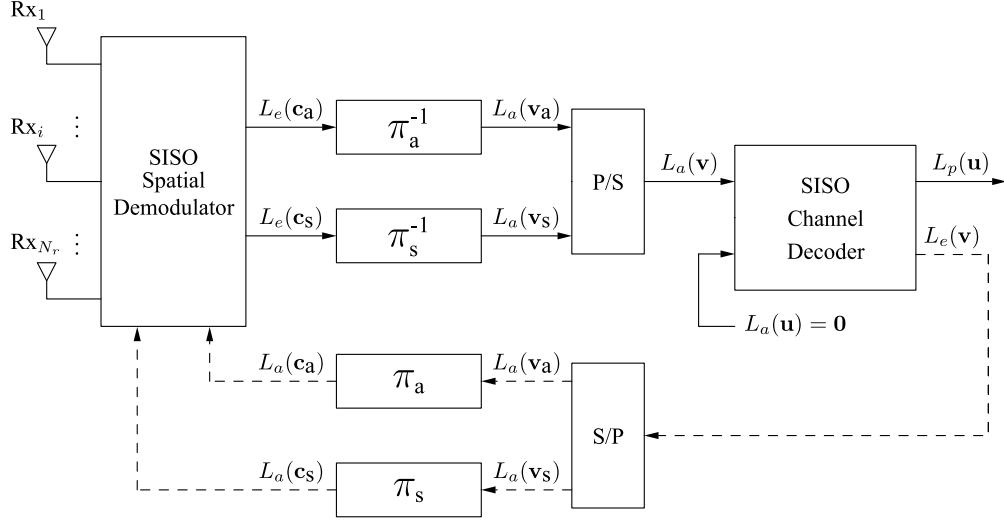


Figure 5.2. Block diagram of SISO BICSM-UEP receiver system.

as,

$$L_p(c_{a,i}) = \log \frac{p(c_{a,i} = 1 | \mathbf{y})}{p(c_{a,i} = 0 | \mathbf{y})} \quad (5.1)$$

$$\begin{aligned} &= \log \frac{\sum_{\mathcal{V}} \sum_{\mathcal{U}_{i,1}} p(\mathbf{y} | \mathbf{h}_u x_v) \prod_{j=1}^n P(c_{a,j})}{\sum_{\mathcal{V}} \sum_{\mathcal{U}_{i,0}} p(\mathbf{y} | \mathbf{h}_u x_v) \prod_{j=1}^n P(c_{a,j})} \\ &= \log \frac{\sum_{\mathcal{V}} \sum_{\mathcal{U}_{i,1}} e^{-\rho |\mathbf{y} - \mathbf{h}_u x_v|^2 + \sum_{j=1}^n \log P(c_{a,j})}}{\sum_{\mathcal{V}} \sum_{\mathcal{U}_{i,0}} e^{-\rho |\mathbf{y} - \mathbf{h}_u x_v|^2 + \sum_{j=1}^n \log P(c_{a,j})}} \end{aligned}$$

$$\begin{aligned} L_p(c_{s,i}) &= \log \frac{p(c_{s,i} = 1 | \mathbf{y})}{p(c_{s,i} = 0 | \mathbf{y})} \quad (5.2) \\ &= \log \frac{\sum_{\mathcal{U}} \sum_{\mathcal{V}_{i,1}} e^{-\rho |\mathbf{y} - \mathbf{h}_u x_v|^2 + \sum_{j=1}^m \log P(c_{s,j})}}{\sum_{\mathcal{U}} \sum_{\mathcal{V}_{i,0}} e^{-\rho |\mathbf{y} - \mathbf{h}_u x_v|^2 + \sum_{j=1}^m \log P(c_{s,j})}} \end{aligned}$$

Where $P(\cdot)$ denotes the priori probabilities.

5.2. Simulation Results for Soft Decision Decoding

In this section BICSM-EPP and BICSM-UEP systems are designed with various code rates and with soft decision decoding. The performance curves are plotted with Monte Carlo simulation technique for uncorrelated/correlated Rayleigh and uncorrelated/correlated Rician channels.

For all simulations SM system with 4 transmit and 4 receive antennas is considered. The overall system spectral efficiency is fixed to 4 b/s/Hz in UEP and EEP to better compare BER performances. For each case every 4 bits are encoded and coded bits are mapped to antenna indexes and symbol constellations. Gray mapping is assumed for bit to symbol mappings. In BICSM-EEP system modulation size is chosen with the corresponding coding rates 64 QAM for $R = 1/2$, 32 QAM for $R = 4/7$, 16 QAM for $R = 4/6$, 8 PSK for $R = 4/5$ respectively. In BICSM-UEP system antenna and symbol bits are encoded separately and antenna bits are always encoded with rate $R = 1/2$ convolutional encoder. Symbol bits coding rate and corresponding modulation alphabet size is 32 QAM for $R = 3/5$, 16 QAM for $R = 3/4$ and 8 PSK for uncoded symbol case. In uncoded symbol case, incoming three bits are directly mapped to 8 PSK constellation without encoding. Channel is modelled by the general channel model in Section 2.2, where Rayleigh and Rician channels can be modelled with appropriate parameter selection. For all Rician channels Rician coefficient K is chosen 3. The channel correlations are modelled by exponential correlation model in Section 3.1, where transmitter and receiver correlations chosen to model strong correlation with $\alpha_t = 0.8$ and $\alpha_r = 0.8$ respectively. For both BICSM-EEP and BICSM-UEP systems rate $R = 1/2$ convolutional code with $(5, 7)_8$ generator is used to obtain punctured codes. All codes used in BICSM-EEP and BICSM-UEP systems are chosen best codes from Table 4.1 and Table 4.3, respectively. Decoding of all convolutional codes are done by soft decision decoder employing MAP [37] algorithm.

Additionally, performance curve of uncoded SM system is also provided to compare with coded performance improvement. Uncoded scheme is employing 4 transmit antenna and QPSK modulation to achieve 4 b/s/Hz spectral efficiency. All curves are drawn down to at least 1×10^{-5} BER levels.

BICSM-EEP/UEP performance plots for Rayleigh fading channels are shown in Figure 5.3. Among the other EEP schemes, two bit punctured code plot with rate $R = 4/6$ and 16 QAM modulation perform best in uncorelated Rayleigh fading channel. One can observe that, this best performing scheme is the same as in the hard decoded case and at 1×10^{-5} BER level soft decision decoding case perform 4 dB better

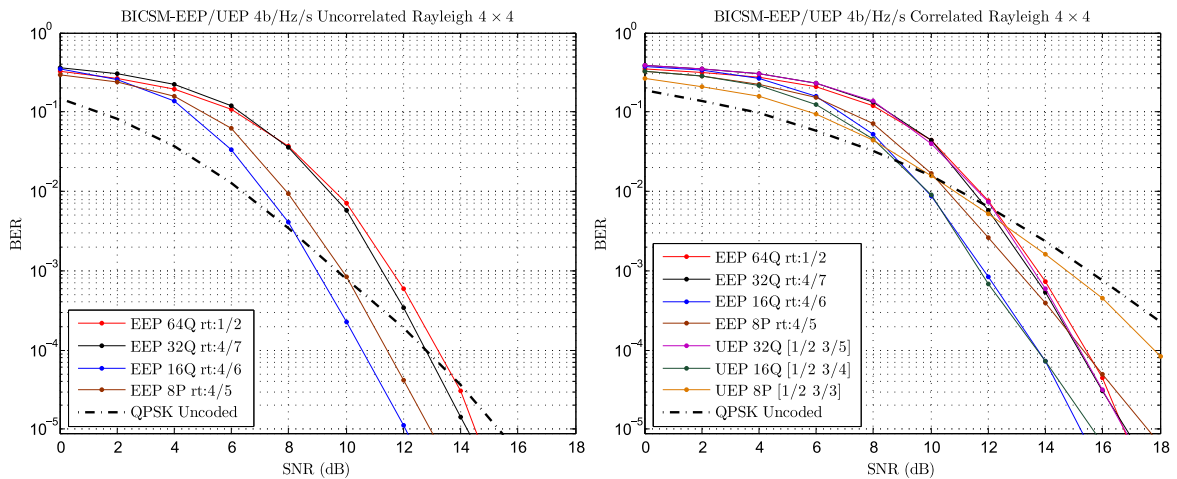


Figure 5.3. Soft Decoded Rayleigh Fading Channels with various puncturing pattern.

than hard decoded case. In correlated Rayleigh fading channel UEP scheme with rate $R = [1/2 \ 3/4]$ with 16 QAM symbol constellation and EEP scheme with rate $R=4/6$ and 16 QAM are the best performing schemes. Although punctured codes have weak error protection capability, this superior performances can be explained by utilization of smaller constellation size. UEP scheme with rate $R = [1/2 \ 3/4]$ with 16 QAM perform 3 dB better at 1×10^{-5} BER level compared to hard decoded case.

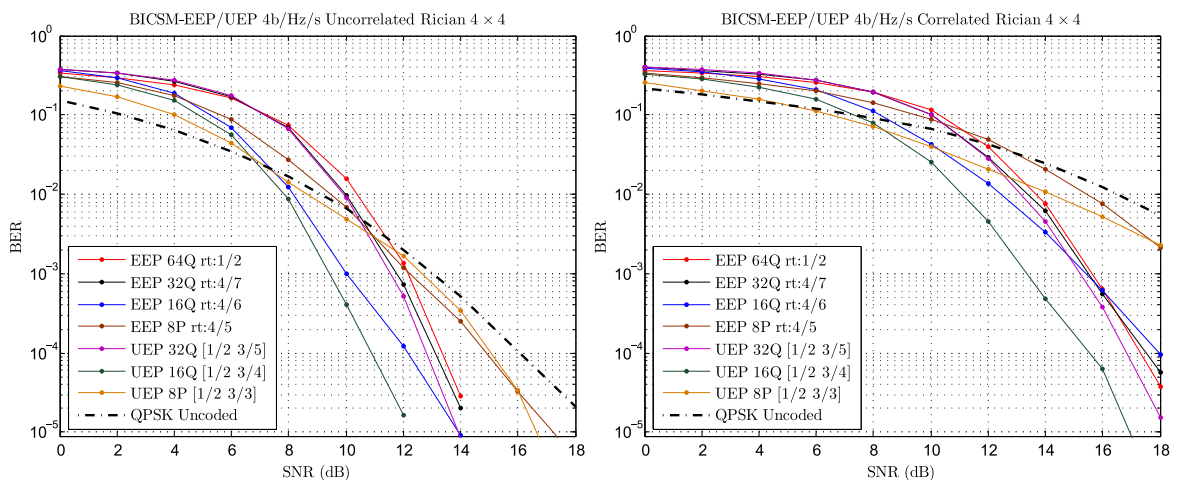


Figure 5.4. Soft Decoded Rician Fading Channels with various puncturing pattern.

In Figure 5.4 performance curves for EEP and UEP schemes are plotted for uncorrelated/correlated Rician channels. Similar to hard decoded case, UEP scheme with rate $R = [1/2 \ 3/4]$ and 16 QAM has best performance in both channel types. At 1×10^{-5} BER level there is 5 dB performance improvement compared to uncoded case in uncorrelated Rician channel. As one may notice, distinctively from hard de-

coded case, UEP scheme with $R = [1/2 \ 3/5]$ 32 QAM performances are following performances of best performing UEP $R = [1/2 \ 3/4]$ 16 QAM. This can be explained as performance improvement caused by reduced constellation size significantly surpass performance degradation caused by punctured convolutional codes. And this result in overall performance improvement.

In conclusion, for all BICSM EEP/UEP schemes great performance improvement can be achieved by implementing soft decision decoding compared to hard decision decoding. In addition, advantage of using UEP strategy is more obvious in soft decision decoding for correlated and Rician channel types since the effect of greater euclidean distance is more influential.

6. CONCLUSION

SM is novel modulation technique that utilize antenna space in addition to symbol space for information transmission. Performance improvement and robustness over this system can be obtained by employing BICM and designing coding and modulation together. This thesis focus on problems of how much coding required for antenna and symbol bits and how equal or unequal coding strategies can be implemented and perform on different channel conditions. Additionally, system design and optimization with code selection mechanism is also investigated.

Firstly, antenna and symbol bit error probabilities are compared via simulation in uncoded case. And new performance metric P_b^a/P_b^s is derived to find amount of required protection for antenna and symbol bits. This metric is a useful tool to observe effect of channel impairments such as Rician factor, channel correlation on antenna and symbol bits. Use of this metric gives an insight for how the system should be designed in different channel conditions.

The second focus of this thesis is on system design and performance evaluation. An analytical upper bound for performance comparison is developed for both EEP and UEP systems with hard decision decoding. This upper bounding technique is greatly simplified performance evaluation process and abolish the need on Monte Carlo simulations that take long time. Derived bound is relatively tight especially in the high SNR region. As a future work this upper bounding technique can be extended for performance evaluation of BICSM system with soft decision decoding.

Punctured convolutional codes are another focus of this thesis since they are one of the key feature of both BICSM-EEP and BICSM-UEP systems. By using developed upper bounding technique, system performances with various code rates and puncturing patterns are compared and optimum performing codes with their weight distributions are tabulated.

Optimum punctured convolutional codes used in system desing, which is also in focus of this thesis. Various UEP and EEP schemes are designed for correlated-uncorrelated Rayleigh and correlated-uncorrelated Rician channels. Performance of designed schemes are compared and importance of unequal protection is validated once again for correlated and Rician channels. Obtained results are fully compatible with previously made observations with metric P_a/P_s . BICSM-UEP system can achieve good BER performance with employing punctured convolutional codes. While puncturing decrease performance of convolutional code, coded bits can be mapped to smaller symbol constellations that result in performance improvement since euclidean distance between symbol pairs is increased. Among these two counteracting phenomena, upon careful selection of coding scheme, performance improvement can be achieved when increased euclidean distance effect overcome the degradation caused by puncturing. As a future work bit to symbol mappings on BICSM system design can be investigated. Bit to symbol labelling has important effect in conventional BICM system and it may also be a system design parameter for BICSM.

REFERENCES

1. Di Renzo, M., H. Haas, A. Ghayeb, S. Sugiura and L. Hanzo, “Spatial Modulation for Generalized MIMO: Challenges, Opportunities, and Implementation”, *Proceedings of the IEEE*, Vol. 102, No. 1, pp. 56–103, Jan 2014.
2. Mesleh, R. Y., H. Haas, S. Sinanovic, C. W. Ahn and S. Yun, “Spatial Modulation”, *IEEE Transactions on Vehicular Technology*, Vol. 57, No. 4, pp. 2228–2241, July 2008.
3. Mesleh, R., H. Haas, C. W. Ahn and S. Yun, “Spatial Modulation - A New Low Complexity Spectral Efficiency Enhancing Technique”, *2006 First International Conference on Communications and Networking in China*, pp. 1–5, Oct 2006.
4. Mietzner, J., R. Schober, L. Lampe, W. H. Gerstacker and P. A. Hoeher, “Multiple-antenna techniques for wireless communications - a comprehensive literature survey”, *IEEE Communications Surveys Tutorials*, Vol. 11, No. 2, pp. 87–105, 2009.
5. Jeganathan, J., A. Ghayeb, L. Szczecinski and A. Ceron, “Space shift keying modulation for MIMO channels”, *IEEE Transactions on Wireless Communications*, Vol. 8, No. 7, pp. 3692–3703, 2009.
6. Jeganathan, J., A. Ghayeb and L. Szczecinski, “Spatial modulation: optimal detection and performance analysis”, *IEEE Communications Letters*, Vol. 12, No. 8, pp. 545–547, 2008.
7. Renzo, M. D., H. Haas and P. M. Grant, “Spatial modulation for multiple-antenna wireless systems: a survey”, *IEEE Communications Magazine*, Vol. 49, No. 12, pp. 182–191, 2011.
8. Younis, A., N. Serafimovski, R. Mesleh and H. Haas, “Generalised spatial modulation”, *2010 Conference Record of the Forty Fourth Asilomar Conference on Signals,*

- Systems and Computers*, pp. 1498–1502, 2010.
9. Di Renzo, M. and H. Haas, “Performance Comparison of Different Spatial Modulation Schemes in Correlated Fading Channels”, *2010 IEEE International Conference on Communications*, pp. 1–6, 2010.
 10. Peng, S., Z. Bai, Y. Su, S. Sun, T. Han and K. Kwak, “MRC based SER analysis of high efficient UWB spatial modulation system”, *2017 13th International Wireless Communications and Mobile Computing Conference (IWCMC)*, pp. 1712–1716, 2017.
 11. Bai, Z., S. Peng, Q. Zhang and N. Zhang, “OCC-Selection-Based High-Efficient UWB Spatial Modulation System Over a Multipath Fading Channel”, *IEEE Systems Journal*, Vol. 13, No. 2, pp. 1181–1189, 2019.
 12. Mesleh, R., H. Elgala and H. Haas, “Optical Spatial Modulation”, *IEEE/OSA Journal of Optical Communications and Networking*, Vol. 3, No. 3, pp. 234–244, 2011.
 13. Basar, E., U. Aygolu, E. Panayirci and H. V. Poor, “Space-Time Block Coded Spatial Modulation”, *IEEE Transactions on Communications*, Vol. 59, No. 3, pp. 823–832, 2011.
 14. Di Renzo, M. and H. Haas, “Performance analysis of Spatial Modulation”, *2010 5th International ICST Conference on Communications and Networking in China*, pp. 1–7, 2010.
 15. Koca, M. and H. Sari, “Performance Analysis of Spatial Modulation over Correlated Fading Channels”, *2012 IEEE Vehicular Technology Conference (VTC Fall)*, pp. 1–5, 2012.
 16. Alshamali, A. and B. Quza, “Spatial modulation: Performance evaluation in Nakagami fading channels”, *2009 5th IEEE GCC Conference Exhibition*, pp. 1–4, 2009.

17. Ganesan, S., R. Mesleh, H. Ho, C. W. Ahn and S. Yun, “On the Performance of Spatial Modulation OFDM”, *2006 Fortieth Asilomar Conference on Signals, Systems and Computers*, pp. 1825–1829, 2006.
18. Mesleh, R., M. D. Renzo, H. Haas and P. M. Grant, “Trellis Coded Spatial Modulation”, *IEEE Transactions on Wireless Communications*, Vol. 9, No. 7, pp. 2349–2361, 2010.
19. Basar, E., U. Aygolu, E. Panayirci and H. V. Poor, “New Trellis Code Design for Spatial Modulation”, *IEEE Transactions on Wireless Communications*, Vol. 10, No. 8, pp. 2670–2680, 2011.
20. Koca, M. and H. Sari, “Bit-interleaved coded spatial modulation”, *2012 IEEE 23rd International Symposium on Personal, Indoor and Mobile Radio Communications - (PIMRC)*, pp. 1949–1954, 2012.
21. Ungerboeck, G., “Channel coding with multilevel/phase signals”, *IEEE Transactions on Information Theory*, Vol. 28, No. 1, pp. 55–67, 1982.
22. Zehavi, E., “8-PSK trellis codes on Rayleigh channel”, *IEEE Military Communications Conference, 'Bridging the Gap. Interoperability, Survivability, Security'*, pp. 536–540 vol.2, 1989.
23. Alvarado, A., E. Agrell, L. Szczecinski and A. Svensson, “Exploiting UEP in QAM-based BICM: interleaver and code design”, *IEEE Transactions on Communications*, Vol. 58, No. 2, pp. 500–510, 2010.
24. Xiaodong Li and J. A. Ritcey, “Bit-interleaved coded modulation with iterative decoding”, *1999 IEEE International Conference on Communications (Cat. No. 99CH36311)*, Vol. 2, pp. 858–863 vol.2, 1999.
25. Xiaodong Li and J. A. Ritcey, “Trellis-coded modulation with bit interleaving and iterative decoding”, *IEEE Journal on Selected Areas in Communications*, Vol. 17,

- No. 4, pp. 715–724, 1999.
26. Caire, G., G. Taricco and E. Biglieri, “Bit-interleaved coded modulation”, *IEEE Transactions on Information Theory*, Vol. 44, No. 3, pp. 927–946, 1998.
 27. Huang, L., W. Sheen and T. Yu, “A Tight BER Upper Bound for Bit-Interleaved Coded Modulation with Square QAM and Gray Labeling”, *IEEE Transactions on Wireless Communications*, Vol. 5, No. 11, pp. 2983–2987, 2006.
 28. Szczecinski, L., R. Bettancourt and R. Feick, “Probability Density Function of Reliability Metrics in BICM with Arbitrary Modulation: Closed-form through Algorithmic Approach”, *IEEE Transactions on Communications*, Vol. 56, No. 5, pp. 736–742, 2008.
 29. Martinez, A., A. Guillen i Fabregas and G. Caire, “Error probability analysis of bit-interleaved coded modulation”, *IEEE Transactions on Information Theory*, Vol. 52, No. 1, pp. 262–271, 2006.
 30. Martinez, A., A. Guillen i Fabregas and G. Caire, “Bit-Interleaved Coded Modulation”, *Foundations and Trends® in Communications and Information Theory*, Vol. 5, No. 1–2, pp. 1–153, 2008.
 31. Szczecinski, L. and A. Alvarado, *Bit Interleaved Coded Modulation*, Wiley, 2015.
 32. Tuchler, M., “Design of serially concatenated systems depending on the block length”, *IEEE Transactions on Communications*, Vol. 52, No. 2, pp. 209–218, 2004.
 33. Di Renzo, M. and H. Haas, “Bit Error Probability of SM-MIMO Over Generalized Fading Channels”, *IEEE Transactions on Vehicular Technology*, Vol. 61, No. 3, pp. 1124–1144, 2012.
 34. Neeser, F. D. and J. L. Massey, “Proper complex random processes with applica-

- tions to information theory”, *IEEE Transactions on Information Theory*, Vol. 39, No. 4, pp. 1293–1302, 1993.
35. Alouini, M. . and A. J. Goldsmith, “A unified approach for calculating error rates of linearly modulated signals over generalized fading channels”, *IEEE Transactions on Communications*, Vol. 47, No. 9, pp. 1324–1334, 1999.
 36. Loyka, S. L., “Channel capacity of MIMO architecture using the exponential correlation matrix”, *IEEE Communications Letters*, Vol. 5, No. 9, pp. 369–371, 2001.
 37. Lin, S. and D. J. Costello, *Error Control Coding*, Prentice-Hall, 1983.
 38. Cain, J., G. Clark and J. Geist, “Punctured convolutional codes of rate $(n-1)/n$ and simplified maximum likelihood decoding (Corresp.)”, *IEEE Transactions on Information Theory*, Vol. 25, No. 1, pp. 97–100, 1979.
 39. Yasuda, Y., K. Kashiki and Y. Hirata, “High-Rate Punctured Convolutional Codes for Soft Decision Viterbi Decoding”, *IEEE Transactions on Communications*, Vol. 32, No. 3, pp. 315–319, 1984.
 40. Hole, K. J., “New short constraint length rate $(n-1)/n$ punctured convolutional codes for soft-decision Viterbi decoding”, *IEEE Transactions on Information Theory*, Vol. 34, No. 5, pp. 1079–1081, 1988.
 41. Begin, G. and D. Haccoun, “High-rate punctured convolutional codes: structure properties and construction technique”, *IEEE Transactions on Communications*, Vol. 37, No. 12, pp. 1381–1385, 1989.
 42. Hagenauer, J., “Rate-compatible punctured convolutional codes (RCPC codes) and their applications”, *IEEE Transactions on Communications*, Vol. 36, No. 4, pp. 389–400, 1988.
 43. Frenger, P., P. Orten, T. Ottosson and A. Svensson, *Multi-rate Convolutional*

Codes, Tech. rep., Chalmers U.T, 1998.

44. Haccoun, D. and G. Begin, “High-rate punctured convolutional codes for Viterbi and sequential decoding”, *IEEE Transactions on Communications*, Vol. 37, No. 11, pp. 1113–1125, 1989.
45. *Punctured Convolutional Codes*, <http://itpp.sourceforge.net/4.3.1/>, accessed in June 2019.